



EXPERIMENTAL RESULTS

CHAPTER 5

Analysis of GaN cleaning procedures

5.1 Introduction

A number of groups have investigated GaN cleaning procedures for device fabrication [1-5]. The importance of properly cleaned surfaces for ohmic and Schottky contacts deposition is well known [4-5]. There is currently no standard method of preparing the GaN substrate prior to metallization. Preparation methods differ from one laboratory to the other. Wet and dry etching methods are widely used in surface preparation for removal of surface contaminants. In addition, the morphology of the surface of the substrate prior to metallization has an influence on the continuity of the ultra-thin metals used in fabrication of Schottky barrier diodes for ultraviolet (UV) detection. Wet and dry cleaning of substrates using chemicals have been used on GaN prior to metallization. Dry cleaning methods are known for introducing damage to the surface, usually making the material electrically unsuitable [6]. Various surface analytical techniques such as Auger electron spectroscopy (AES), x-ray photoelectron spectroscopy (XPS), low energy electron diffraction (LEED), and secondary ion mass spectroscopy (SIMS) have been used to identify the surface contaminants, oxides, metal particulate and reconstruction. Atomic force microscopy (AFM) has been used to monitor the surface cleanliness as a function of topography [7, 8].

The work done by Smith et al. in cleaning GaN has shown that the choice of cleaning chemical is of utmost importance [1]. In their work, they used AES to compare HCl and HF based solutions in methanol and in water, to remove contaminants on the GaN surface. The use of UV/O₃ treatment was also done. All the chemical cleaning was followed by thermal desorption at temperatures of up to 800°C to completely produce a contamination free surface. From their results, it was observed that dissolving HCl in deionised water (DI) resulted in cleaner surfaces as compared to dissolving in methanol. HF results showed that C (carbon) and O (oxygen) residues were lower in HF:DI solution than in HF:methanol solution. These results were

influenced by the physisorption of methanol, thus increasing C content on the surface of GaN. Comparing HCl:DI and HF:DI, it was found that HF based solution was more effective in removing both C and O on the surface. A further observation was the presence of Cl on the surface after treatment with HCl based solution and UV/O₃ increased the surface oxide while decreasing the C. The best cleaning method according to Smith et al. is the final step in which HF was diluted in deionised water as it removed most of the C, O and Cl without leaving any traces of F on the surface. The thermal desorption results showed further reduction of C and O as the temperature is gradually increased up to 800°C, beyond which the decomposition of GaN was observed.

Further work done by King et al. using XPS and AES, on both AlN and GaN showed that different chemicals may be used to yield atomically clean surfaces [2]. They used HCl, HF, NH₄F, HNO₃, H₂SO₄, H₃PO₄, H₂O₂, NH₄OH, NaOH, KOH, RCA SC1 and SC2 (1:1:5NH₃OH: H₂O₂: H₂O at 85°C and 1:1:5 HCl:H₂O₂: H₂O at 85°C) and TCE, acetone, methanol and UV/O₃ treatment. Thermal desorption was done in an integrated UHV system at temperatures of up to 1100°C. As in the previous work by King et al. UV/O₃ was found to be effective in removing C and simultaneously increasing O on the surface. In addition to reducing the C peak, the exposure to UV/O₃ moved the C peak to higher energies, consistent with oxidation of C species on the surface of GaN. It was observed that increasing ozone concentration further reduced C on the surface though it was not completely removed. Further observations of the UV/O₃ exposed surface, showed an increase in the rate of oxidation of GaN surface, as seen in complete disappearance of N KLL and N1s peaks. The observed oxides were found to be in the form of Ga₂O₃ and N-O at binding energies 20.8 and 398.2 eV respectively.

The use of HCl, NH₄OH and HF solutions were found to effectively remove the oxides. A 1:1 HCl:DI solution was found to produce the lowest C/N ratio with a disadvantage of Cl addition to the surface. The O coverage on the HCl sample was found to be inversely proportional to Cl detected on the surface. According to their results, the fact that the N-Cl bond strength is less than that of Ga-Cl gave an explanation why there is Cl residue on GaN surface. The results of using H₂SO₄ and H₃PO₄ were observed residues of SO₄ and PO₄ on the surfaces of GaN, increasing surface oxide coverage after these treatments. The 1:10 HF-based cleaning solutions

were found to increase the O/N ratio with no detection of F on the surface. Stoichiometric GaN surface was produced after annealing the surfaces at 700 – 800°C in NH₃. Using thermal desorption, it was found that HCl cleaned samples showed complete desorption of all contaminant species on the surface after 950°C. AFM was used to investigate the surface roughness of the cleaned surfaces. All samples had surface RMS roughness comparable with the as grown material, while H₃PO₄ resulted in increased surface roughness from as low as 20 Å to as high as 200 Å. On the GaN surface, the RCA SC1 and SC2 reduced the UV/O₃ oxides, though SC2 left more C on the surface relative to SC1.

Lee et al. investigated several methods of cleaning GaN [3]. The methods included different wet chemical procedures, as well as in-situ cleaning in AES at elevated temperatures. The wet chemical methods consisted of acetone, methanol, HF or HCl and UV/O₃ treatments. Thermal cleaning was done in N₂ and H₂/N₂ plasma. UV/O₃ increased the O on the surface while decreasing the C peak. Using AES, it was observed that the surface of the as-grown (as-received) sample contained about 12% C and 13% O and that the Ga/N ratio was 1.08. Applying photoresist and stripping it with acetone reduced the O content slightly, and increased the carbon content to 30%. Treatment in HCl further reduced the O concentration to 7% and the C content to almost the same level as of the as-grown sample. The HCl treatment also left Cl contamination on the surface. Using thermal cleaning after various chemical treatments reduced the C and O surface content to below the detection limit of AES. AFM results showed insignificant change in surface roughness after all the wet chemical cleaning on GaN surface.

The work by Pelto et al. in pre-metallization treatment of GaN for ohmic contacts fabrication showed that the surface cleaning recipes depends on what device is being fabricated [4]. The following etch recipes were used: H₂SO₄: H₃PO₄: DI (1:1:2), HCl:DI (1:2), HNO₃: HCl (1:3), and NH₄OH:DI (1:10). The ohmic contacts' behaviour depended on the etch recipe used, and the expected outcomes. On the other hand, Machuca et al. used a simple cleaning method focusing on the optimization of electron emitters with wide band gap [5]. Using H₂SO₄: H₂O₂ (4:1) to reduce contaminants on GaN surfaces followed by annealing in vacuum at 700°C, they showed that after chemical clean, the vacuum anneal was best for thermal desorption of C and O than

annealing in NH_3 . Both these authors do not comment on any remaining surface contaminants on GaN and their effects on electrical properties of the devices made.

Thermal desorption in the vacuum has been recommended as a final step in most cleaning procedures. In particular, thermal desorption done in vacuum have shown that all the surface contaminants can be reduced to less than the AES detection limit. In the above works done, it can be summarized that thermal desorption of contaminants on GaN is independent of what has been used chemically prior to heating. Heating the material to a temperature range from 800°C to 1000°C has shown complete removal of C all contaminants on GaN surface [1, 2, 3].

The above review shows that there is still a gap in GaN cleaning procedures used prior to metallization. There is a need to test the effects of chemical cleaning procedures by evaluating electrical characteristics of devices. In this work, we have investigated chemical cleaning of GaN surfaces and evaluating the results with AFM and AES. A variety of wet chemistries for O and C removal were investigated. We particularly report on the effects of HCl, KOH and $(\text{NH}_4)_2\text{S}$ on GaN surfaces. In addition we give thermal cleaning results.

5.2 Experimental

n-GaN samples of orientation (1000) and unintentional doping of $1.6 \times 10^{16} \text{cm}^{-3}$ were obtained from AIXTRON, grown by metal organic chemical vapor deposition (MOCVD) on sapphire (Al_2O_3) substrate. The thickness of the GaN layer was $1\mu\text{m}$. The cleaning methods used are summarized in Table 5.1. All samples were finally blown dry with compressed nitrogen gas of ultra-high pure quality. Only analytical grade quality chemicals were used and all water rinses were done in deionised water ($\rho > 18 \text{M}\Omega\cdot\text{cm}$). All samples used in this study were cut from the same wafer for compatibility. Ultrasonic rinse was employed to ensure the removal of all loose debris on the surface. All cleaning equipments used were made of pure quartz glass and Teflon. Samples were loaded into the AES immediately after wet chemical cleaning. AES analysis was carried out on Physical Electronics Model 545 Spectrometer, using a cylindrical mirror analyzer with 5 keV electron beam incident on samples mounted on a sample holder of which the angle with the electron beam is 30° . The percentage surface concentration was calculated from the peak-to-peak heights and relative sensitivity factors for different elements.

Thermal cleaning was done by mounting the degreased sample onto a heater block and loaded into the AES, PHI model 549. The analysis was carried out from room temperature of 23°C, continually monitoring the surface up to a temperature of 1100°C. The heating process was stopped at this stage to avoid any decomposition of GaN into the AES system. The scanning probe microscope used in this study was a commercial instrument model, Topometrix 2000 Discoverer. The topographical features of GaN crystals were studied by means of AFM in contact mode. The 130 μm and 7 μm scanner and standard Topometrix Si_2N_3 tips were applied. All scans were applied under ambient conditions. Several images were taken at different positions on the sample to gain better understanding of the surface topography. The same scan parameters (set point, proportional gain, integral gain and derivative gain) were used, however, in each scan optimizations were performed. The topography of the surfaces were analysed from obtained images, using the surface roughness parameters: the root mean square (RMS) roughness, maximum peak height from the mean line, R_p ; the maximum peak to valley height in the profile, R_t ,

Table 5. 1

Outline of cleaning procedures

Number	Method	Procedure
1	Degrease	Boil in Trichloroethylene for 3 min Boil in Isopropanol for 3 min 3 rinses in DI for 20 sec each Blow dry with N ₂
2	Aqua Regia (AR)	Degrease Boil in HCl:HNO ₃ = 3:1 for 8-10 min 3 rinses in DI for 20 sec each Blow dry in N ₂
3	HCl	Degrease Aquaregia HCl:H ₂ O = 1:1 dip for 60 sec 2 rinses in DI for 20 sec each Blow dry with N ₂
4	KOH	Degrease Aquaregia 1mol KOH boil for 3 min 3 rinses in DI for 60 sec each Blow dry with N ₂
5	(NH ₄) ₂ S	Degrease Aquaregia (NH ₄) ₂ S for 1 min 3 rinses in DI for 60 sec each. Blow dry with N ₂

5.3 Results and Discussion

5.3.1 Atomic Force Microscope

AFM images from randomly selected $5 \times 5 \mu\text{m}^2$ areas of degrease to $(\text{NH}_2)_4\text{S}$ cleaned surfaces and corresponding line profiles are presented in Figure 5.1- 5.5. The images, together with corresponding line profiles, indicate difference in topography of investigated GaN surfaces after every cleaning method. The as grown surface has been degreased to deal with packaging contaminants.

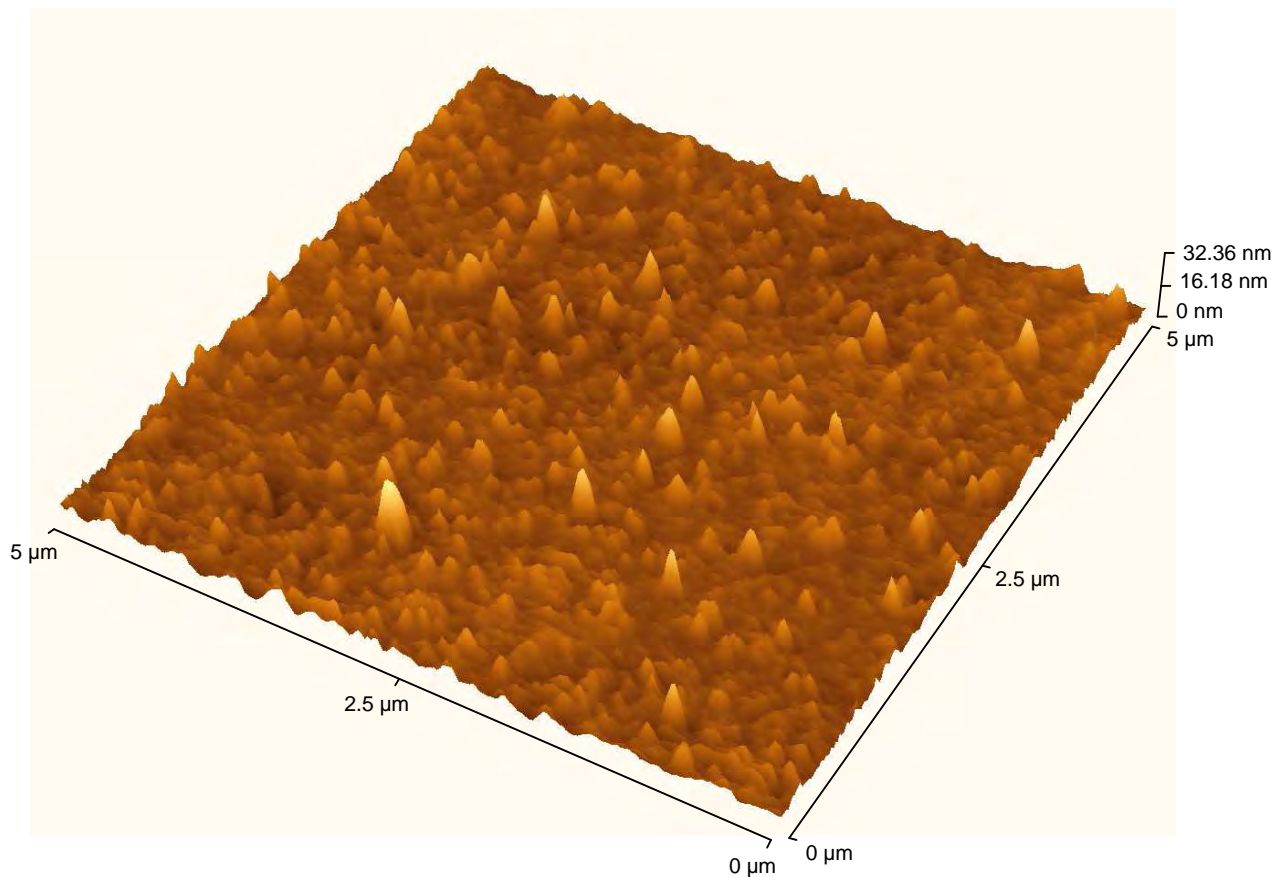


Figure 5.1 (a): AFM images taken from selected degreased $5 \mu\text{m} \times 5 \mu\text{m}$ areas of GaN.

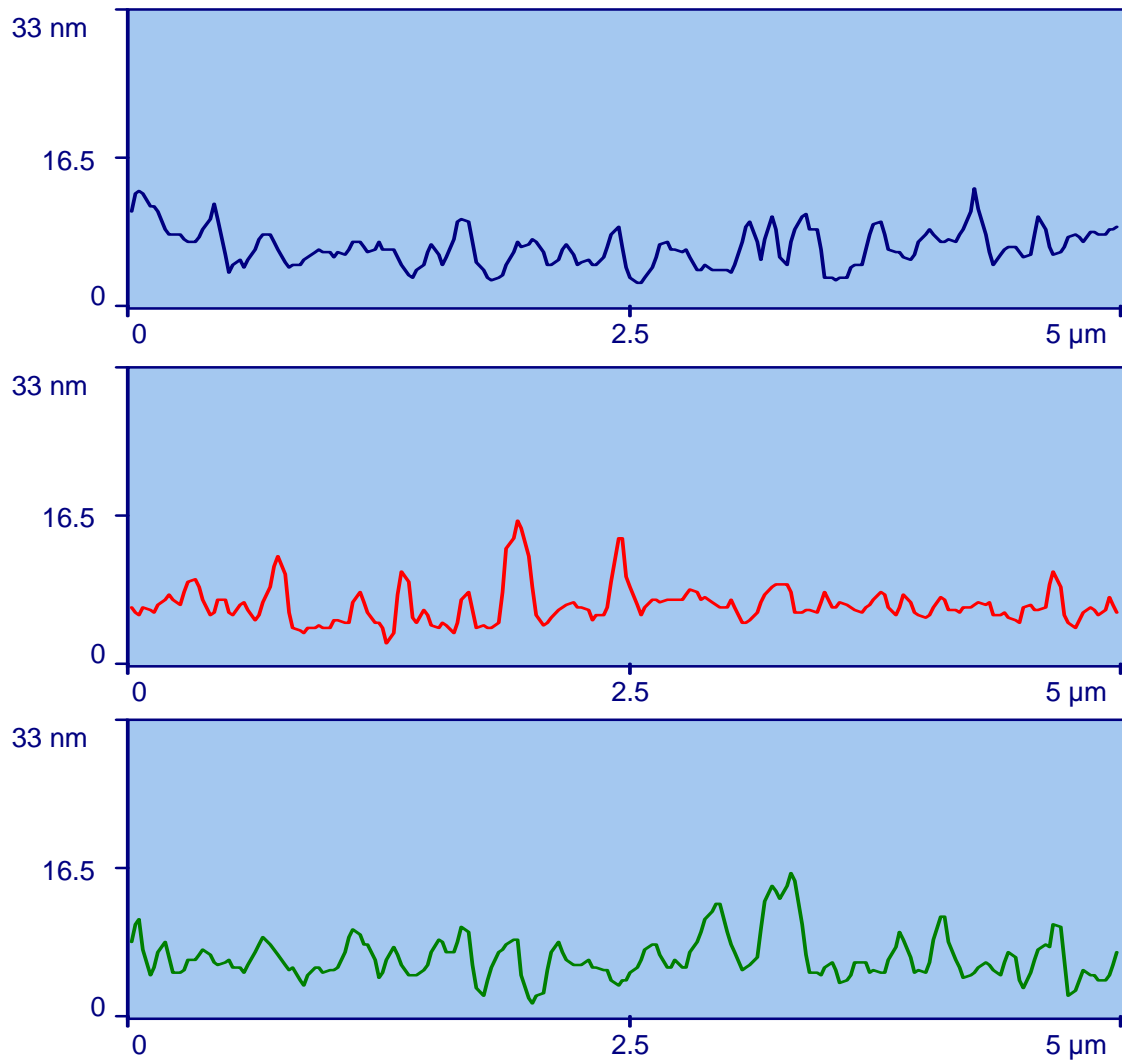


Figure 5.1(b): The corresponding line profiles of AFM images taken from selected degreased 5 μm x 5 μm areas of GaN surfaces cleaned.

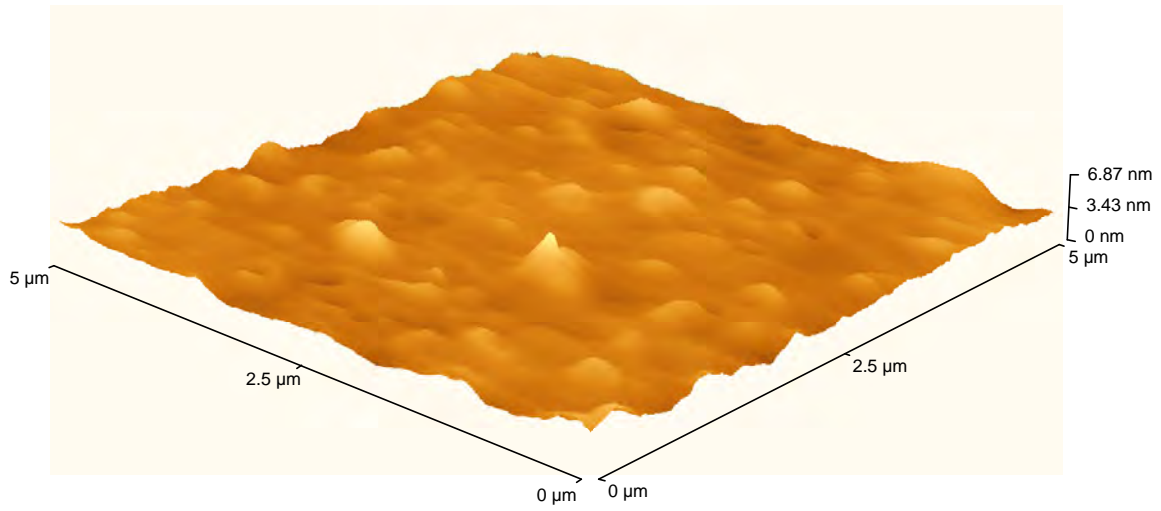


Figure 5.2 (a): AFM images taken from selected aquaregia cleaned 5 μm x 5 μm areas of GaN.

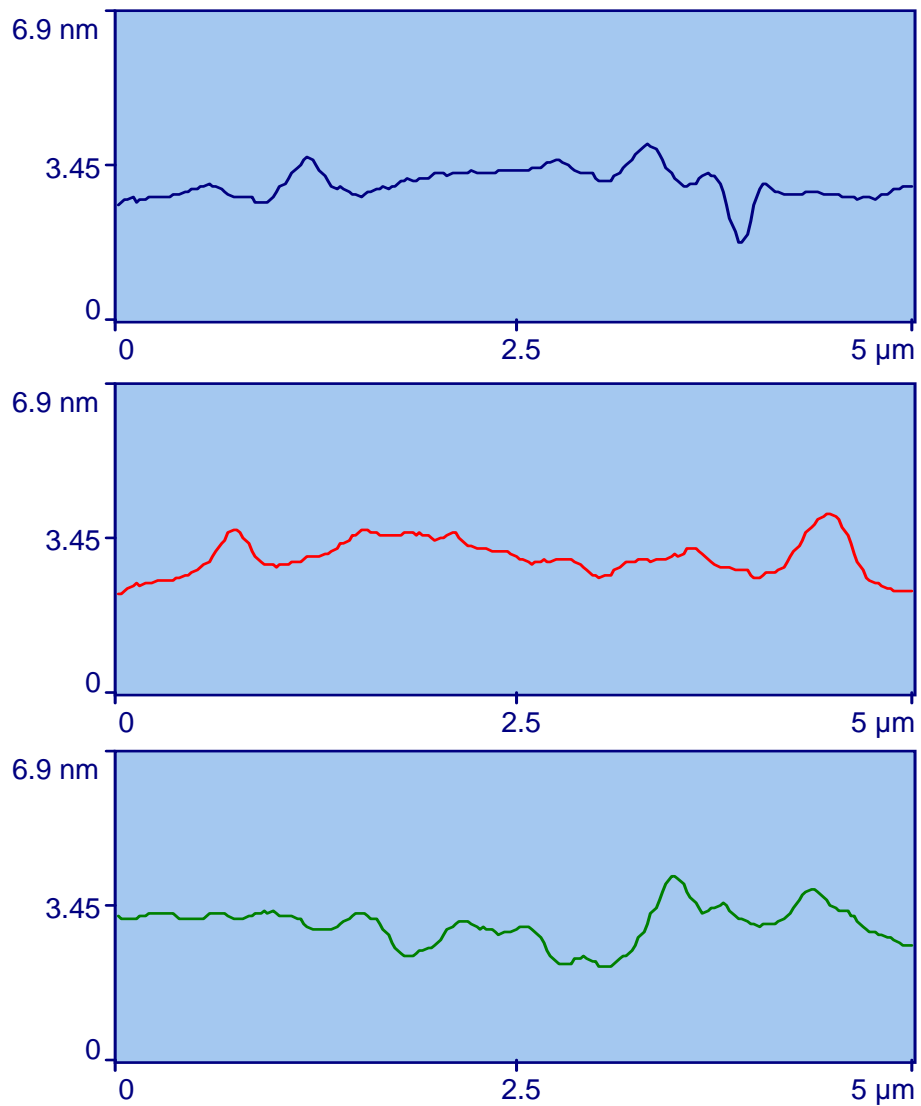


Figure 5.2(b): The corresponding line profiles of AFM images taken from selected aquaregia cleaned 5 µm x 5 µm areas of GaN.

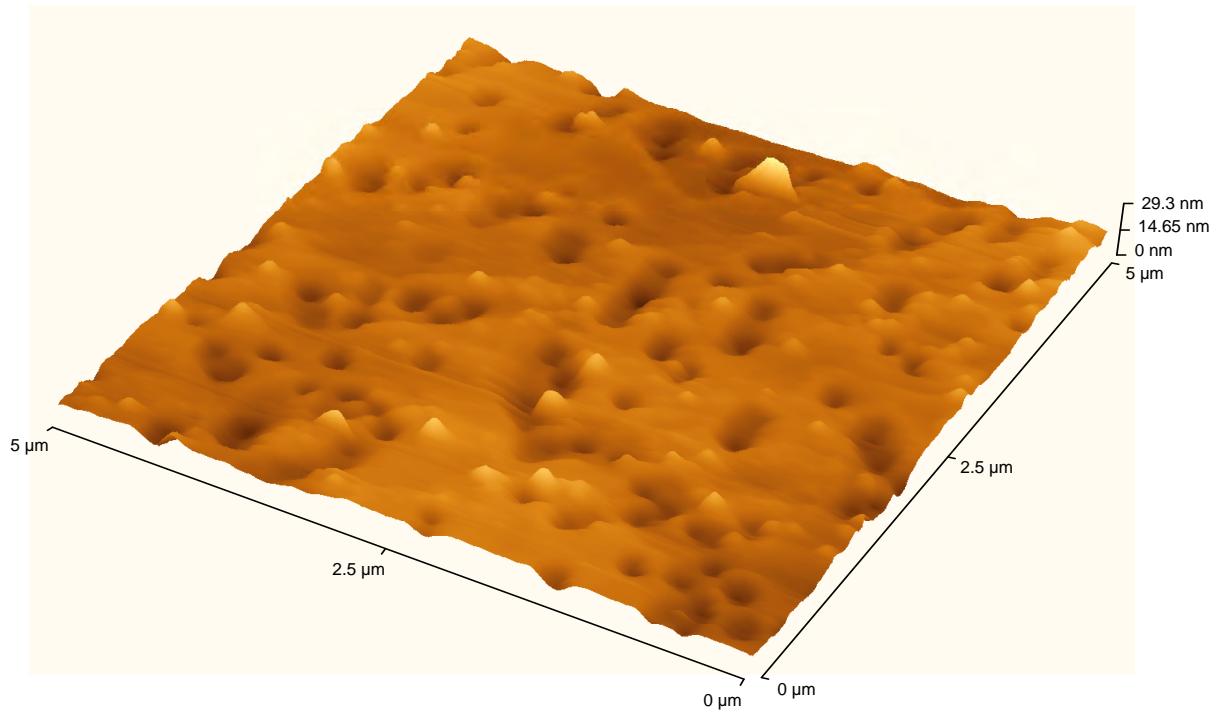


Figure 5.3 (a): AFM images taken from selected HCl cleaned 5 μm x 5 μm areas of GaN.

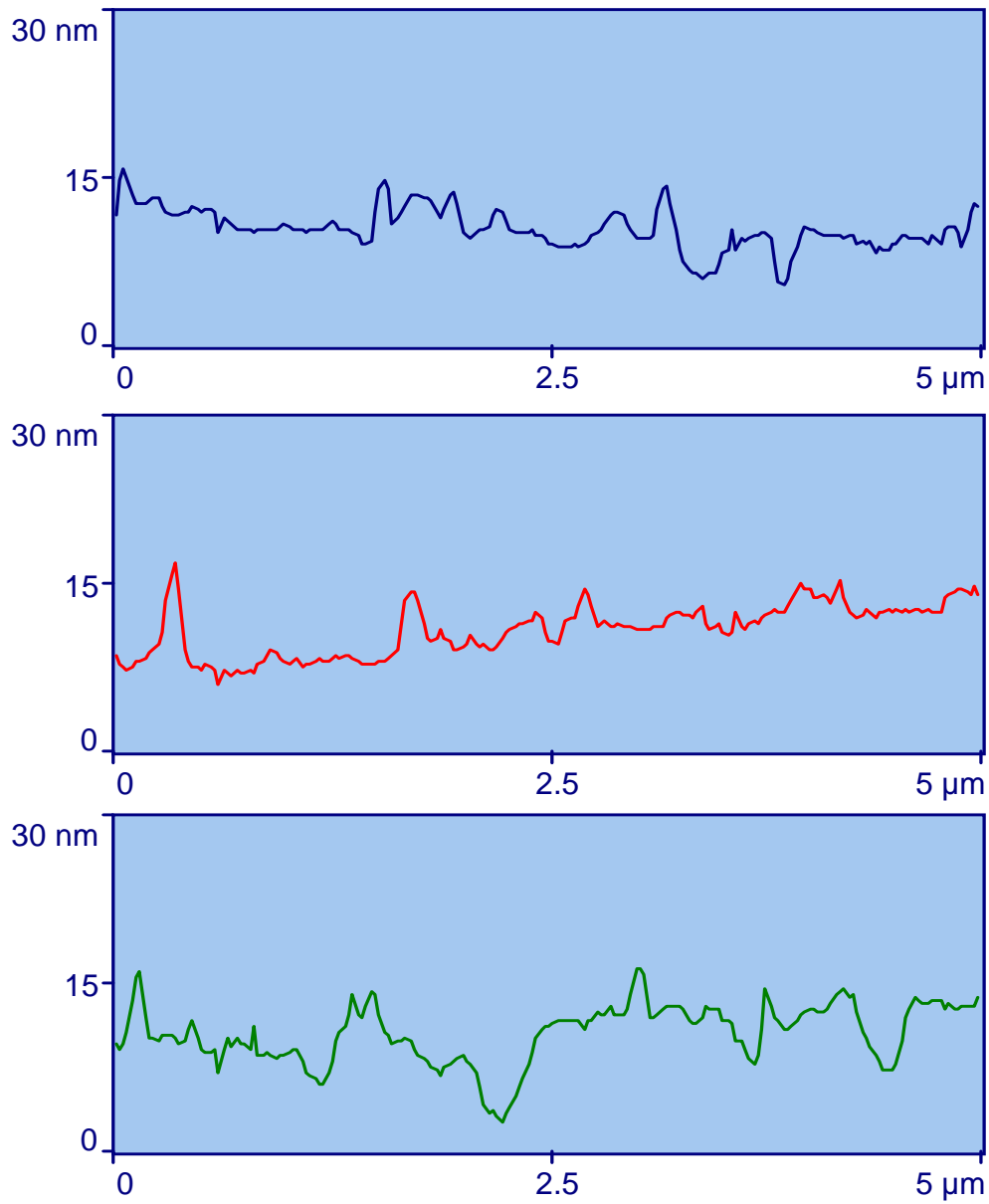


Figure 5.3(b): The corresponding line profiles of AFM images taken from selected HCl cleaned 5 μm x 5 μm areas of GaN.

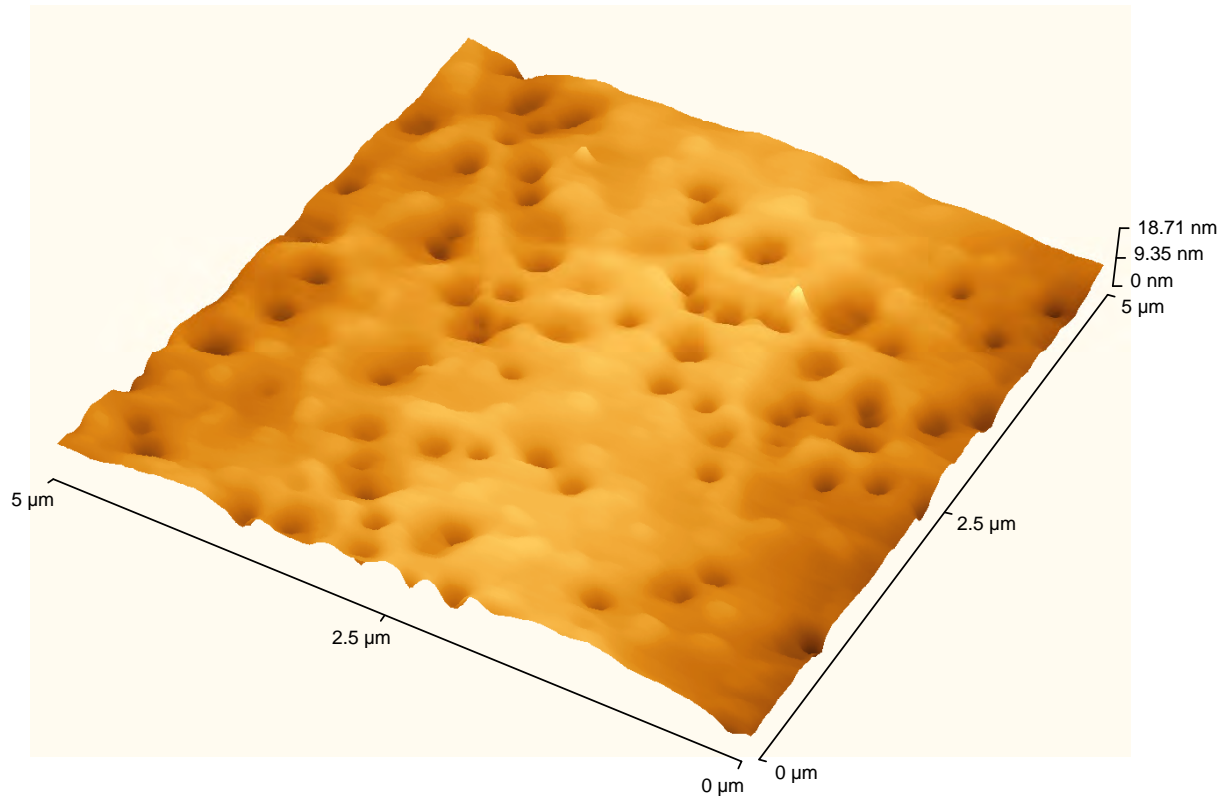


Figure 5.4 (a): AFM images taken from selected KOH etched 5 μm x 5 μm areas of GaN.

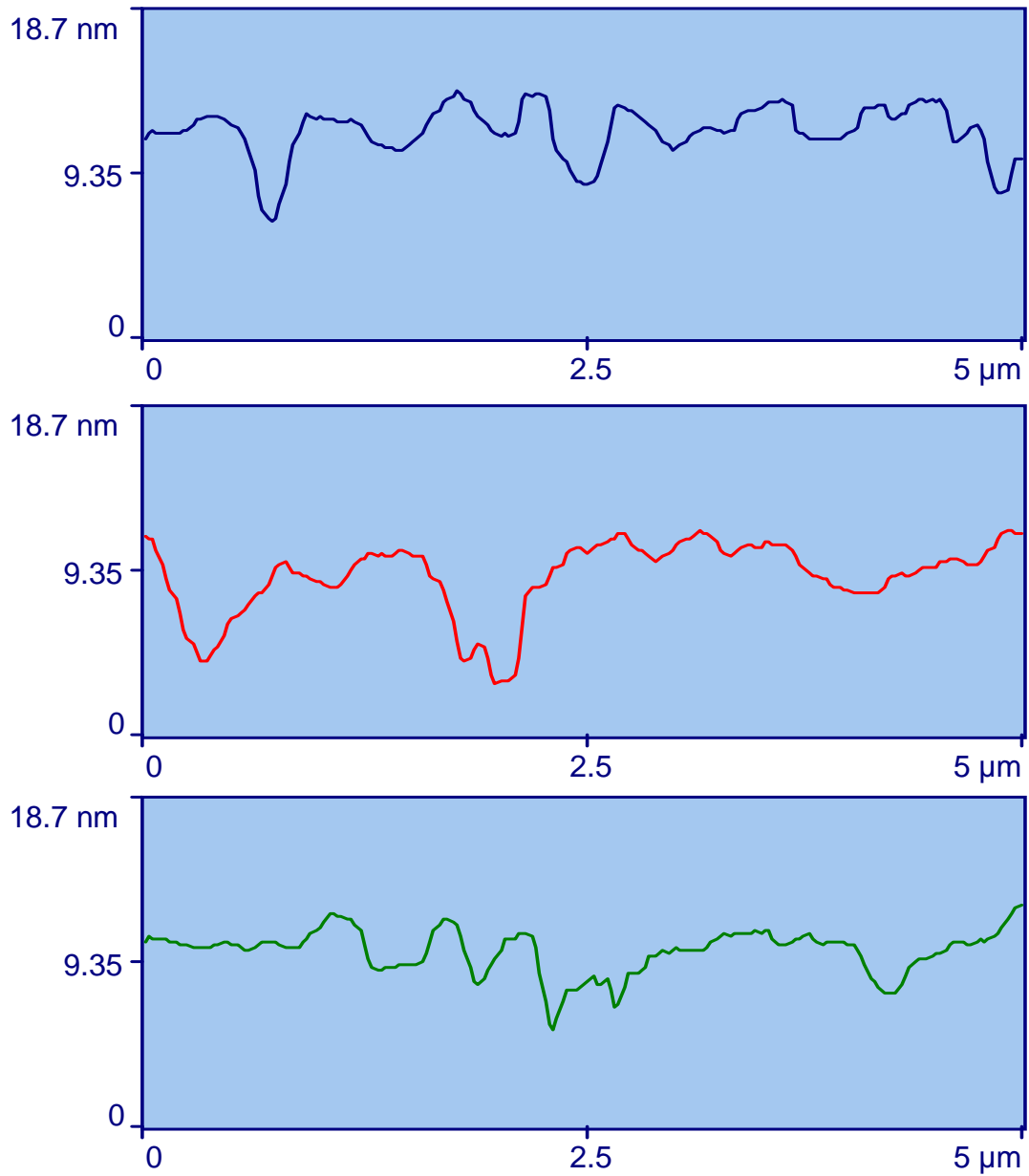


Figure 5.4(b): The corresponding line profiles of AFM images taken from selected KOH etched $5\ \mu\text{m} \times 5\ \mu\text{m}$ areas of GaN.

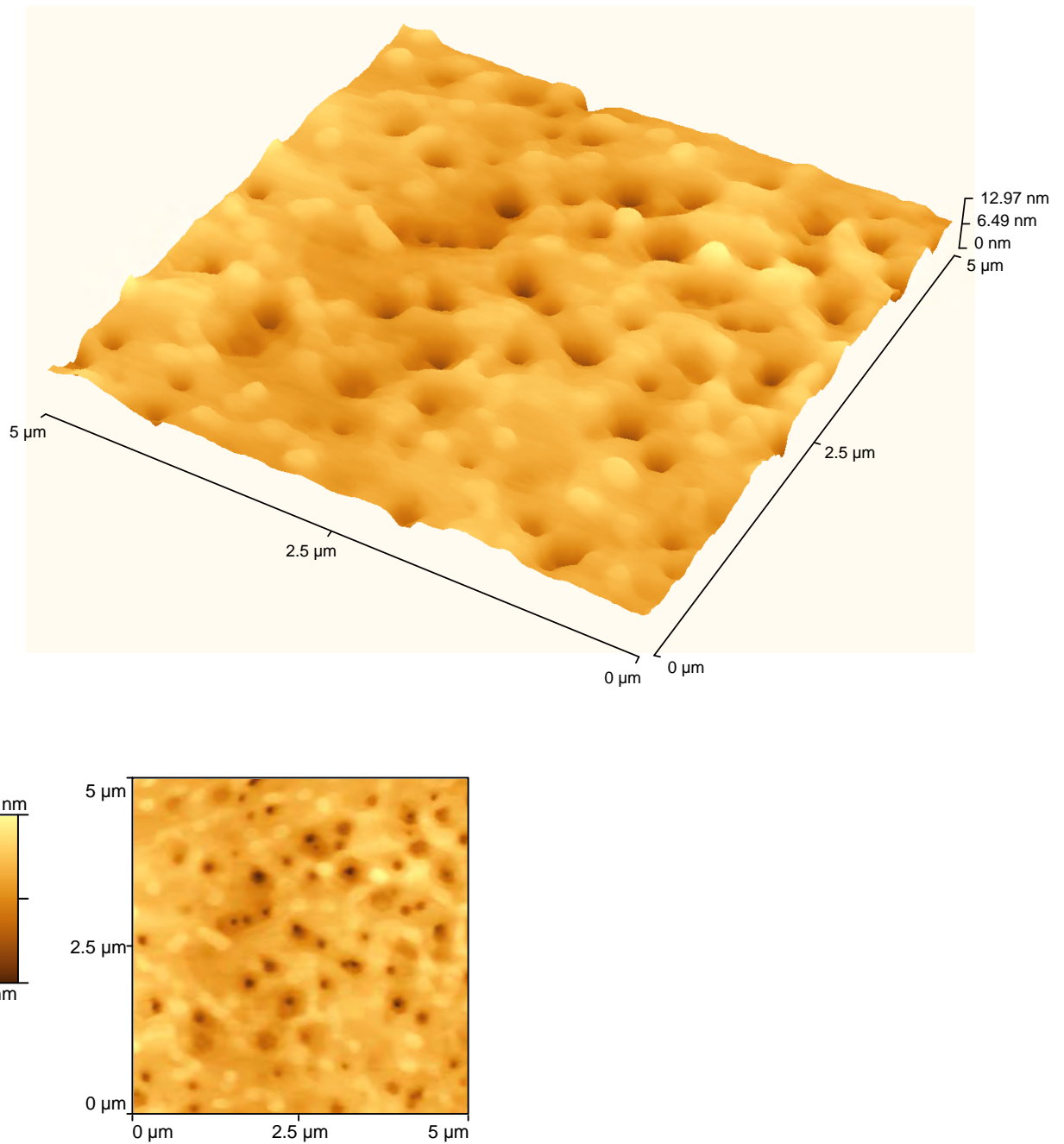


Figure 5.5 (a): AFM images taken from selected $(\text{NH}_4)_2\text{S}$ etched $5 \mu\text{m} \times 5 \mu\text{m}$ areas of GaN and the corresponding flat image.

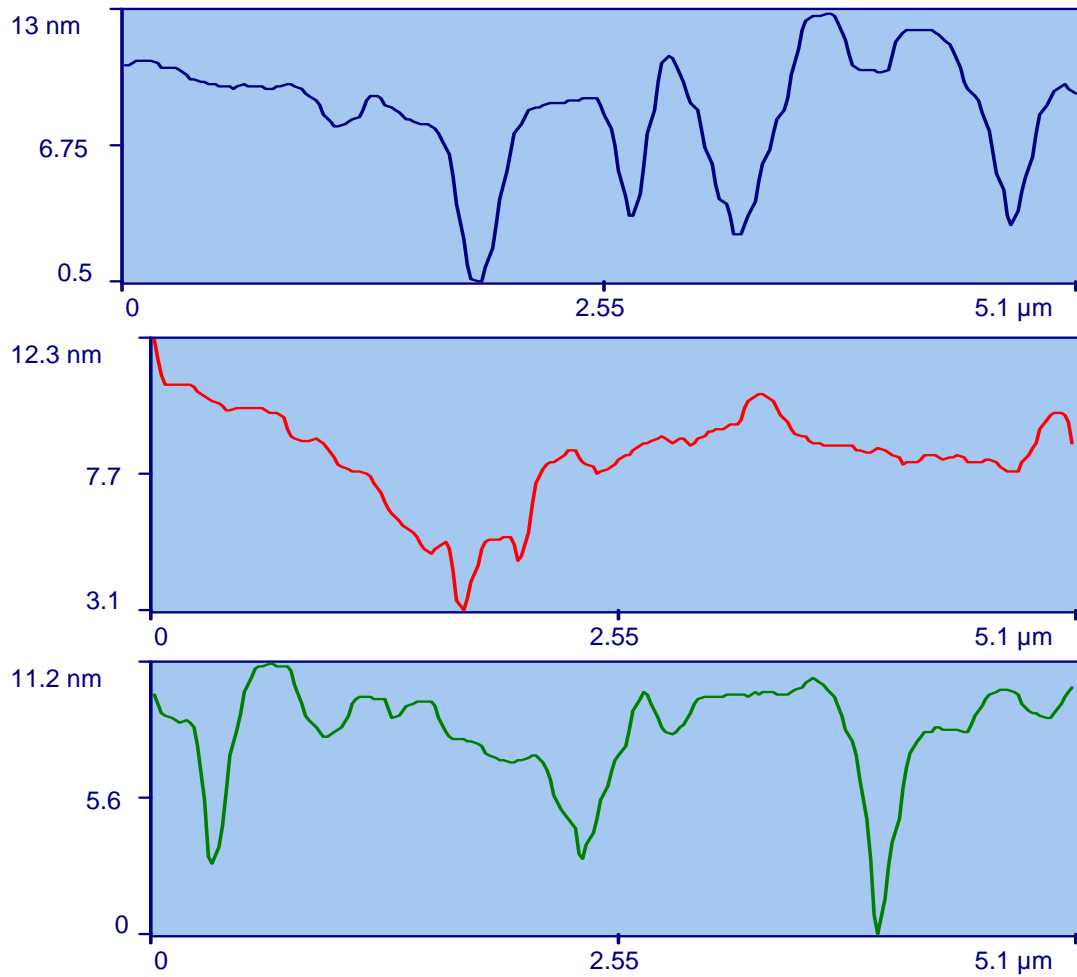


Figure 5.5(b): The corresponding line profiles of AFM images taken from selected $(\text{NH}_4)_2\text{S}$ etched $5 \mu\text{m} \times 5 \mu\text{m}$ areas of GaN.

The as grown surface has needle-shaped protrusion as shown in Figure 5.1(a) and (b) is the corresponding line profile. Using R_t , we compared the difference in features, ranging from protrusions to craters. From R_t measurements, the average height of the protrusions on the surface of the degreased samples was found to be 20.05 nm, as shown in Table 5.2. The second surface, represented in Figure 5.2(a) and (b), was cleaned in aqua regia and shows a disappearance of the protrusions and the emergence of craters, which are hexagonal in shape, with R_t value decreasing to 2.5 nm. This observation implies that the chemicals used thus far, were able to act on the protrusions on the as degreased surface, characterizing GaN by showing hexagonal structure of the crystal.

Table 5.2: Statistical Characterization of GaN samples by AFM.

Cleaning Procedure	Maximum topography variation (R_t -nm)	Mean topography variation (R_p -nm)	RMS surface roughness	Roughness factor
degrease	20.05	11.27	1.74	1.006
aquaregia	2.5	1.55	0.4	1.060
HCl	13.36	7	2.02	1.010
KOH	11.03	4.03	2.1	1.077
(NH ₄) ₂ S	8.74	2.74	1.2	1.098

The next step is etching the surface in HCl, and it is observed that protrusions are disappearing from the surface and craters are increasing, as shown in Figure 5.3(a) and (b). These craters are either isolated or joint to form a bigger crater on the surface and the value of R_t increasing to 13.36 nm, indicating deeper craters as protrusions are removed. The surface protrusions seem to have changed shape, from needles to rounded protrusions. The use of KOH on the surface, as shown in Figure 5.4(a) and (b), shows that the protrusions appeared to be white and flat shaped. In Figure 5.5(a) and (b) the surface of the samples cleaned in (NH₄)₂S are shown. The protrusions on this surface are quite similar to the ones on the KOH etched surface. A two

dimensional (2D) image of the sample cleaned in $(\text{NH}_4)_2\text{S}$ is shown in Figure 5.5 (a), confirming that the observed protrusions on the surface are part of the crystal.

The density of craters on each of the three last cleaning processes is similar, particularly for the HCl and KOH surfaces at approximately $6.2 \times 10^8 \text{ cm}^{-2}$. The $(\text{NH}_4)_2\text{S}$ surface has a little lower density of craters at approximately $5.3 \times 10^8 \text{ cm}^{-2}$. The approximated density of craters is similar to the dislocation density of the GaN used in this experiment, which is approximated to be 10^7 to 10^8 cm^{-2} . Comparing the cleaning procedures, it was found that GaN was etched along the threading dislocation. Threading dislocations have been found to be dominant defects in GaN from TEM studies. In addition, the observed decrease in the density of the craters shows that a new surface has appeared. It has been observed from TEM studies that threading dislocation decrease gradually away from the interface [9]. KOH has been used to characterize defects in GaN, and the defects density was found to be $2 \times 10^9 \text{ cm}^{-2}$. Different values of defect densities have been recorded as $3 \times 10^7 \text{ cm}^{-2}$ and $4 \times 10^7 \text{ cm}^{-2}$ on N-face, and $1 \times 10^7 \text{ cm}^{-2}$ and $5 \times 10^5 \text{ cm}^{-2}$ on Ga-face. The understanding of the mechanisms for the formation thereof, will lead to the reduction of these defects [10].

Using line profiles, statistical parameters were deduced from the AFM for each of the cleaning procedures and are shown in Table 5.2 [11]. From the analysis of these data, the morphologies of differently cleaned surfaces differ from one cleaning method to the other. The value of R_t changed from 20.5 nm for degreased sample to 2.5 nm after aqua regia treated, implying a removal of surface protrusions. The last three etch processes also differ in the value of R_t , indicating how one chemical is able to etch the GaN surface. KOH and $(\text{NH}_4)_2\text{S}$ each were able to produce new surfaces as compared to HCl, which was not able at producing a new surface. The other parameters, R_p , RMS roughness and the roughness factor all confirm the R_t values. The highest RMS roughness is from the KOH etched surface and the lowest is from the aqua regia cleaned surface. Furthermore, using RMS roughness parameter, we have compared the stoichiometries on each of the cleaned surfaces, and stoichiometry and RMS roughness are compared as shown in Figure 5.6.

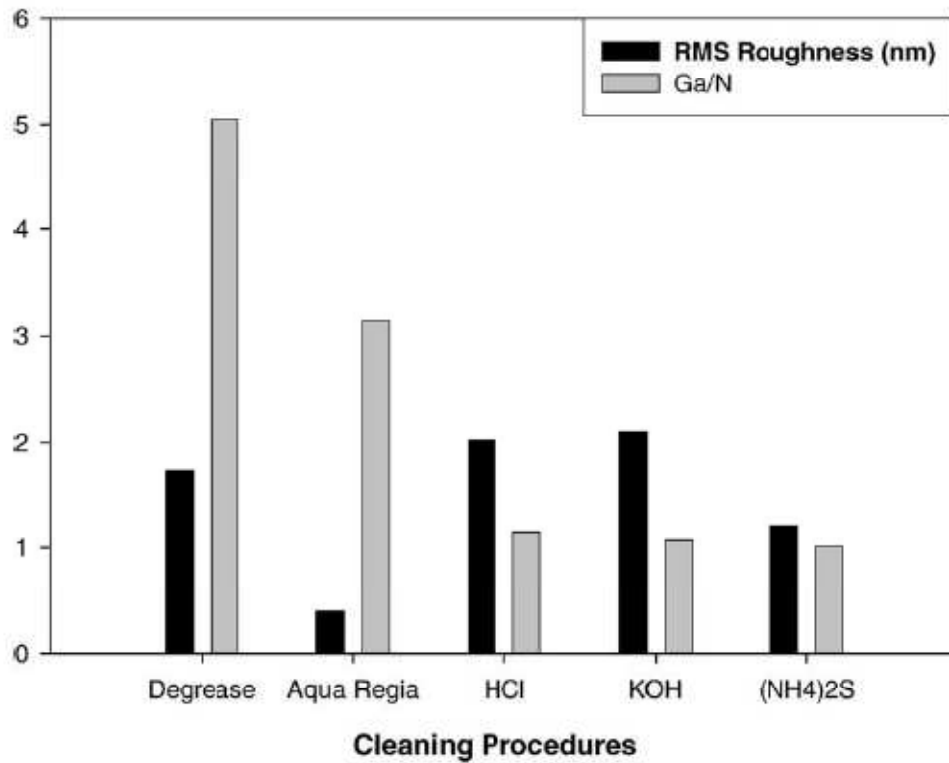


Figure 5.6: Graph of root mean square (RMS) surface roughness and Ga/N ratio from AES elemental surface concentrations.

5.3.2 Auger Electron Spectroscopy

AES was used to analyze the surface contaminants and the results are shown in Figure 5.7. The effect of the cleaning procedure is seen in the reduction of O and C peaks. In addition to reducing C and O peaks, HCl in aqua regia and (NH₄)₂S, respectively, added Cl and S to the surface. The atomic percentage of surface elements present on every surface after wet chemical cleaning procedures was calculated from the relative sensitivity factors. These contaminants may be of advantage to the metal contact formation on the GaN surface as bonding with Au may be enhanced and adhesion improved. Furthermore the use of sulfurants, alkenoids and halogens has proved to enhance adhesion of metals such as Au, Ag, Pt, Pd and Ni to semiconductor surfaces [12,13].

AES surface scans of cleaning procedures

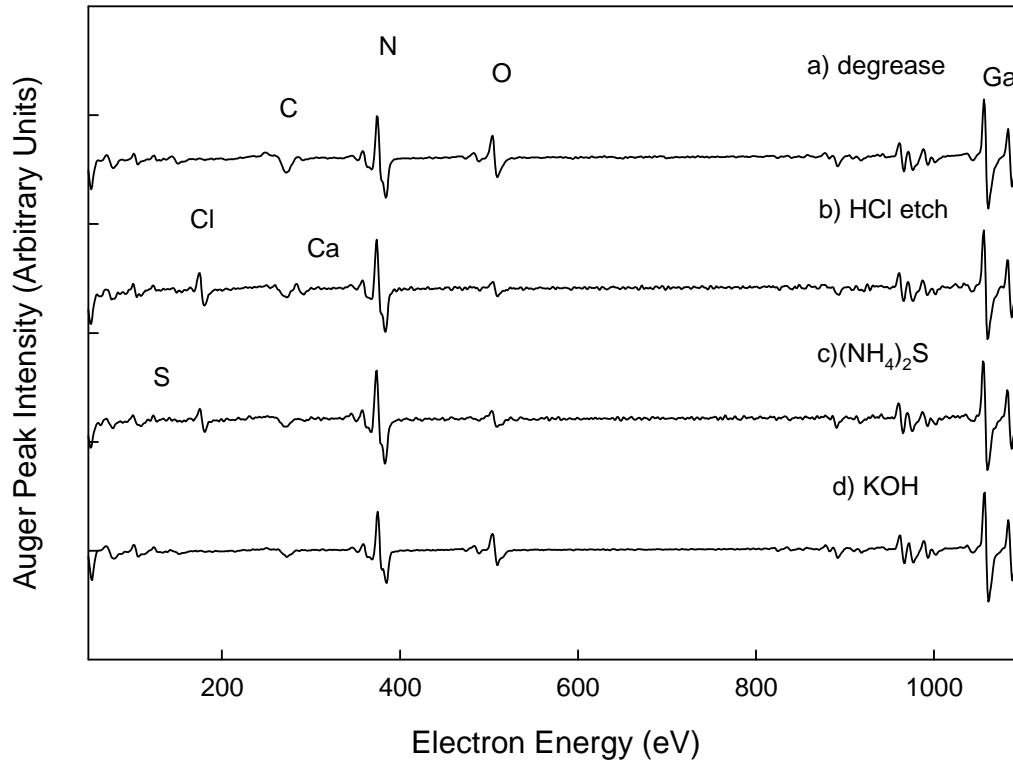


Figure 5.7: AES surface scans of GaN surface cleaned as indicated.

Comparing the AES surface scans of HCl and (NH₄)₂S, it is found that using HCl on the GaN surface reduced the O peak, added Cl, and the use of (NH₄)₂S prevents re-oxidation of the surface, adding insignificant amount of S, and reducing the Cl contaminant. This result further confirms the importance of using (NH₄)₂S as a chemical that prevents re-oxidation of surfaces. KOH removed all the Cl from the surface, and reduced the C significantly.

There had been reports of improved electrical characteristics of metals/GaN contacts after treatments in HF, HCl, and NaOH. E. J. Miller et al has reported the reduction of reverse bias leakage current in GaN Schottky diodes after treatment in NaOH. The high concentration of OH-ion on the GaN surface is attributed to the reduction of reverse bias leakage in their Schottky contacts [14]. In another report, Y-J Lin et al has reported the reduction of surface

states on InGaN using $(\text{NH}_4)_2\text{S}$ [15]. Electrically, $(\text{NH}_4)_2\text{S}$ was reported to reduce the Schottky barrier height. In particular, it was reported that Ga-O, In-O and C-O bonds were removed from the InGaN surface after $(\text{NH}_4)_2\text{S}$ treatment. Furthermore, repeated exposure of the surface that has a Cl peak to the electron beam in the AES system has resulted in desorption of the surface contaminants, and consequently, complete removal of the Cl peak.

To further analyse the cleaned surfaces, the ratio of Ga/N, and RMS surface roughness are plotted as a function of cleaning method, as shown in Figure 5 above. There is a relationship between the RMS surface roughness and the contaminants on the surfaces, which consequently affects the Ga/N ratio. The as grown surface shows a very high surface roughness and Ga/N ratio and the cleanest surface shows lowest surface roughness and Ga/N ratio. Therefore as the surface is cleaned, the surface roughness reduces as the Ga/N ratio improves, implying that the chemicals used has etch GaN surface to removes contaminants. The RMS surface roughness of KOH etched surface, differ from the as grown surface by about 0.4 nm. Different wet chemicals used previously in removing contaminants on GaN have shown no effect on the surface roughness of the material [2,3]. The work done previously to etch and remove surface GaN to form etch steps were not achieved by using HCl and KOH [15]. Ultraviolet light illumination and addition of ions were used to etch GaN successfully in KOH [16].

Previous results have recommended the use of thermal desorption after every chemical clean, to completely remove surface contaminants [1,2,3]. In this work, we have found that thermal cleaning of the degreased GaN surface resulted in almost complete removal of surface contaminants. Figure 5.8 is a typical temperature profile of a sample cleaned in UHV under high temperatures. This profile may be divided into two regions: region I from 23°C to 500°C and region II from 500°C to 1010°C. In region I the carbon peak first decreases and then increases as temperature increases. In region II, the carbon coverage on the surface of GaN decreases until it drops to below AES detection limit, where average peak-to-peak height is less than 1.5. In the case of oxygen, the surface coverage starts increasing and quickly decreases sharply until the temperature of about 500°C. At this temperature, all oxides are removed from the surface according to AES sensitivity, in which average peak-to-peak height is less than 0.5. The increase in O from 23°C to 50°C may be attributed to the removal of common surface water that had been

covering the surface prior to thermal heating. This water is very sticky and is usually removed at temperatures above 220 °C. On the other hand, the increase in C may be due to segregation from the bulk, which needs further study to confirm.

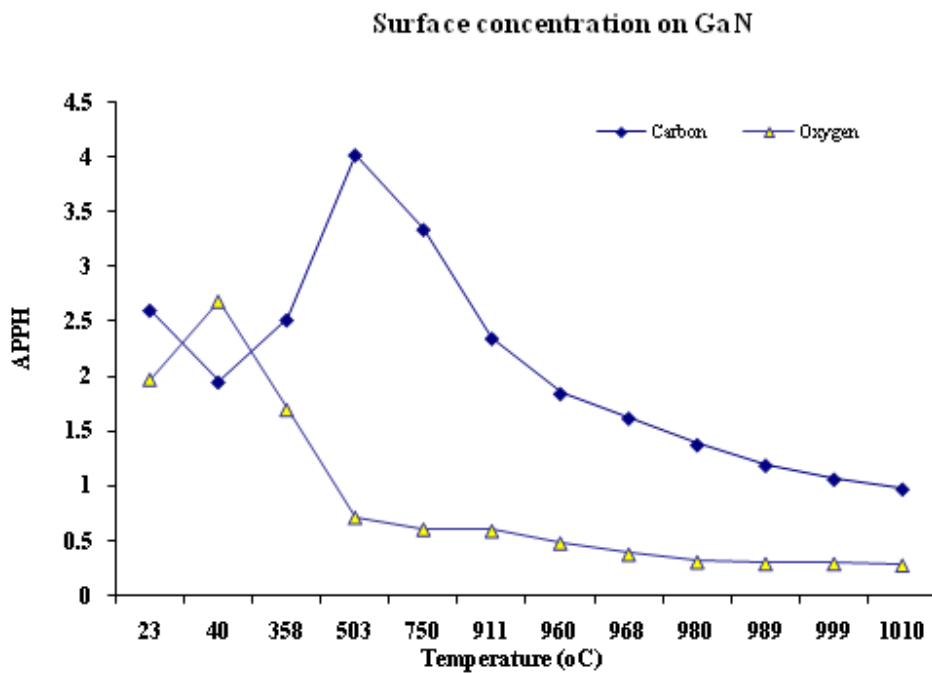


Figure 5.8: Surface concentration profiles of O and C on GaN surface during thermal anneal in the AES.

5.4 Conclusions

In conclusion, the effectiveness of wet chemical cleaning of GaN with different solutions, have been characterized by AFM and AES. AFM results have shown that GaN surface roughness is affected by the cleaning method used on the surface. Surface defects were characterized by different etch chemicals, with $(\text{NH}_4)_2\text{S}$ producing a defects free interface. AES has shown the contaminant as C and O and that using HCl and $(\text{NH}_4)_2\text{S}$, will leave Cl and S on the surface. This result has given sufficient information on removal of surface contamination; stoichiometry; surface roughness and chemical etch. Using $(\text{NH}_4)_2\text{S}$ prevented re-oxidation of the surface, and further removes Cl from the surface of the GaN. KOH effectively removes the C on the surface. The effects of S and Cl on the surface may enhance adhesion of metals to GaN surface, thus improving device quality. Further work is necessary in finding the effects of different cleaning procedures on the optical properties of the material and electrical properties of devices.

REFERENCES

- [1] Smith L. L., King S. W., Nemanich R. J., Davis R. F., *Journal Electronic Materials* **25** (1996) 805.
- [2] King S. W., Barnak J. P., Bremster M. D., Tracey K. M., Ronning C., Davis R. F., Nemanich R. J., *Journal of Applied Physics* **84** (1998) 5248.
- [3] Lee K. N., Donovan S. M., Gila B., Overberg M., Mackenzie J. D., Abernathy C. R., Wilson R. G., *J. Electrochemical Society* **147** (2000) 3087.
- [4] Pelto C. M., Chang Y. A., Chen Y., Williams R. S., *Solid State Electronics* **45** (2001) 1597.
- [5] Machuca F., Liu Z., Sun Y., Pianetta P., Spicer W. E., Pease R. F., *Journal of Vacuum Science and Technology A* **20** (2002) 1784.
- [6] Shul R. J., Vawter G. A., Willison C. G., Lee J. W., Pearton S. J., Abernathy C. R., *Solid State Electronics* **42** (1998) 2259.
- [7] Nel J. M., Demanet C. M., Hillie K. T., Auret F. D., Gaiger H. L., *Applied Surface Science* **134** (1998) 22.
- [8] Deenapanray P. N. K., Auret F. D., Myburg G., Hillie K. T., Demanet C. M., *Surface and Interface Analysis*, **26** (1998) 748.
- [9] Jasinki J., Swider W., Liliental-Werber Z., Visconti P., Jones K. M., Reshchikov M. A., Yun F., Morkoc H., Park S. S., Lee K. Y., *Applied Physics Letters* **78** (2001) 2297.
- [10] Morkoc H., *Materials Science and Engineering* **R33** (2001) 135.
- [11] Zymierska D., Auleytner J., Kobiela T., Dus R., *Physica Status Solidi(a)* **180** (2000) 479.
- [12] Wang J., Zeng B., Fang C., Zhou X., *Journal of Electroanalytical Chemistry* **484** (2000) 88.
- [13] Shalish I., Shapira Y., Burstein L. and Salzan J., *Journal of Applied Physics* **89** (2001) 390.

CHAPTER 6

Experimental Results

Study of metal contacts on GaN for transmission of UV light

6.1 Introduction

Schottky barrier metal-semiconductor contacts are a choice device for the fabrication of ultraviolet [1]. They have simple fabrication technology; suffer lower breakdown voltages, have larger leakage currents at lower voltages as compared with p-n structures of the same semiconductor material. Thus the formation of Schottky contact with high barrier height, low leakage current [2], and good thermal stability [3] to withstand high temperature processing and operation are some of the most important factors in improving the performance of Schottky barrier photodiodes to be used for ultraviolet detection.

Different metals have been used for the formation of such contacts, including Au, Ni and Ni/Au. Sheu et. al. have discovered the high transparency of Ni/Au contacts to GaN, using the metal structure for ohmic contacts to p-GaN. After annealing the contacts at 550 °C, they recorded a transmittance of above 80 %, after forming NiO [4]. NiO is a transparent wide bandgap semiconductor which is very easy to fabricate by annealing Ni in air or in oxygen. This semiconductor is p-type with a bandgap of 4.3 eV [5]. NiO has been used to study the electrical properties of oxidized Au/NiO_x/p-GaN ohmic contact and found that annealing this structure is the main mechanisms that is responsible for the ohmic contact nature of the system [6]. Furthermore, NiO/ZnO structure has been used to study the defects in ZnO [7]. The optical transmittance of 5 nm Au and Ni ultra-thin films is less than 40 % [8]. In this work, we report on the study of Au, Ni, and Ni/Au contacts onto GaN for the fabrication of ultraviolet detectors.

6.2 Choice of metal for transparent contacts

In fabricating UV detectors of Schottky type to GaN, the metal contact must be transparent to UV light. Published works have used a metal layer of high work function and 10 nm thickness onto GaN [2]. A computer modeling program was used, employing the knowledge of the absorption coefficient of GaN and the metal thickness. UV light was focused onto metal/GaN structure and the transmission percent of the structure as a function of UV wavelength range from 240 to 400 nm was recorded. The choice of the metals was due to high work function and availability. Metals with high work function produce high barrier height for Schottky diodes onto semiconductors. Figure 6.1 show the simulation results of the designed metal/GaN photodiodes using different metals. The result of the model made Ag, Au, Ni suitable candidates for fabrication of UV detectors. Ag was abandoned as it was oxidizing easily.

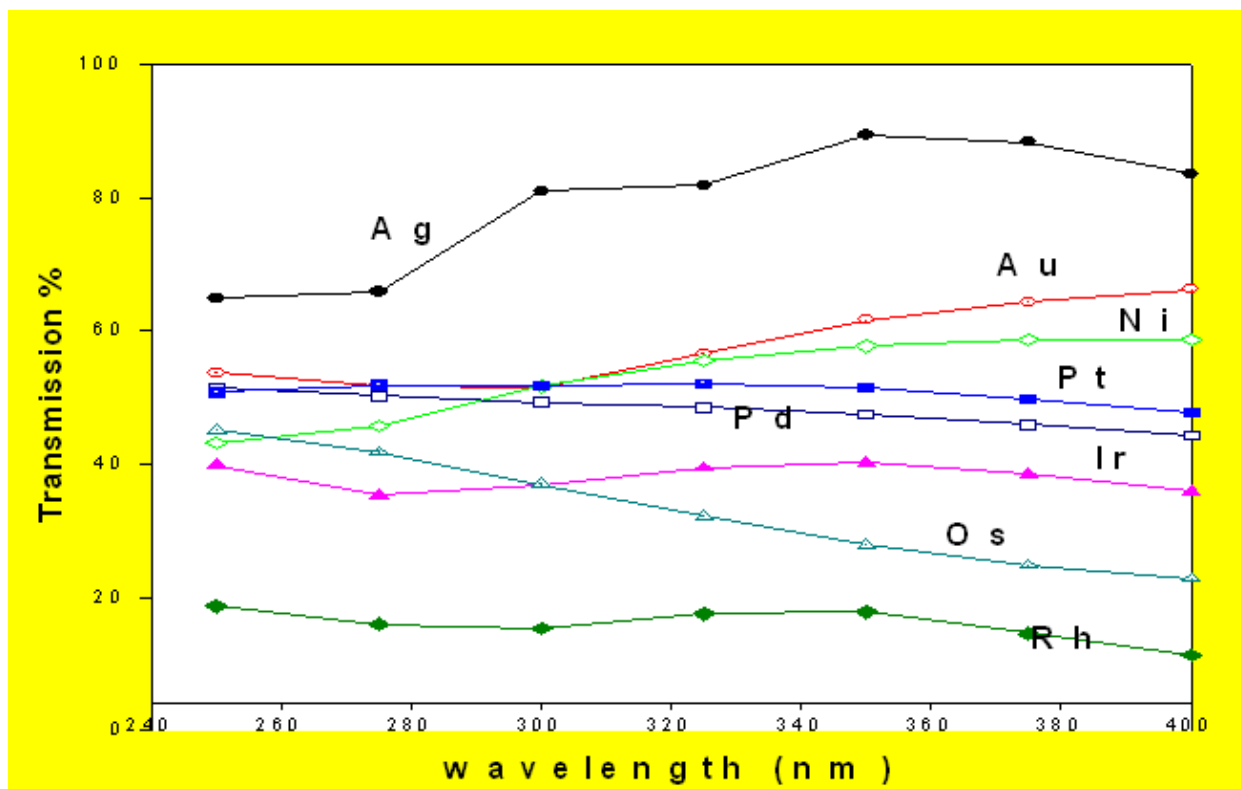


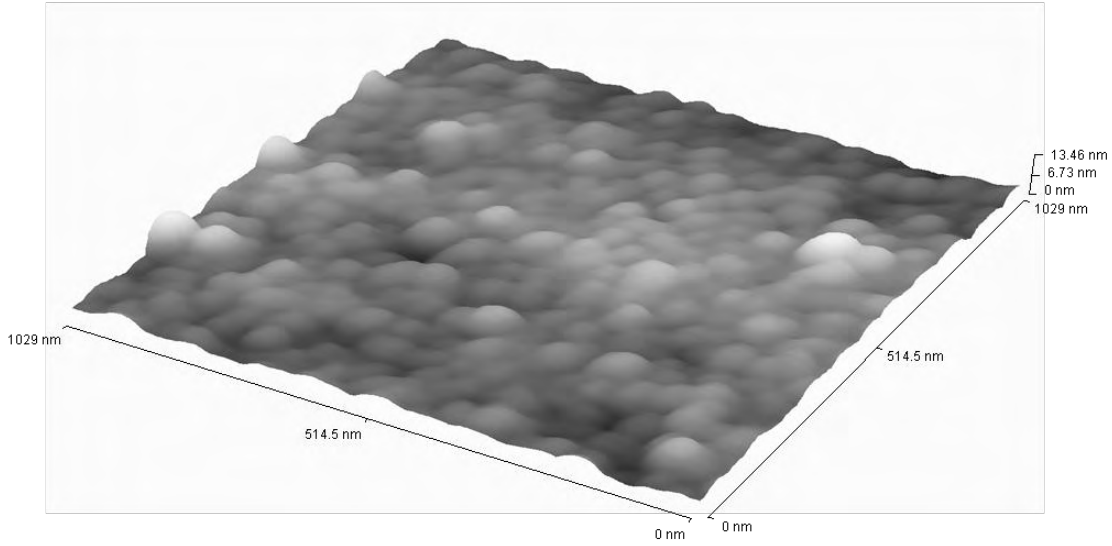
Figure 6.1: Simulation results for the designed metal/GaN photodetector, with Au being highly transparent.

6.3 Experimental

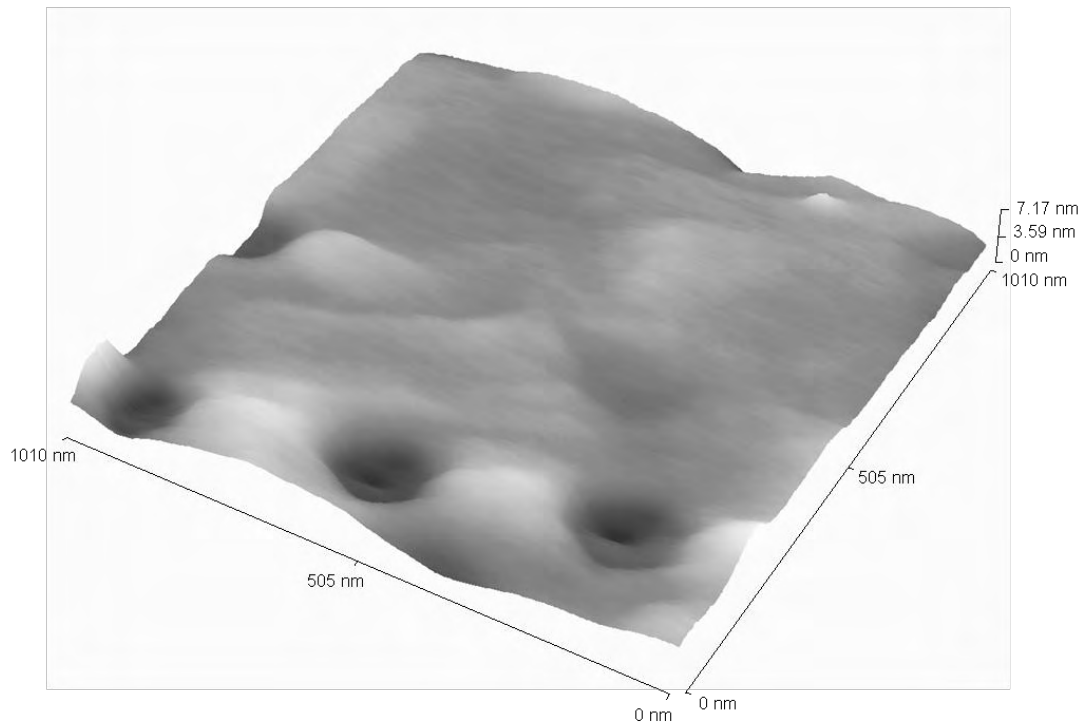
GaN samples were degreased in trichloroethylene and isopropanol; then boiled in aquaregia and finally etched in HCl: H₂O (1:1). Ti/Al/Ni/Au (15 nm /220 nm /40 nm /50 nm) ohmic contacts were electron-beam deposited onto samples and annealed at 500 °C for 5 minutes in air. Circular Au, Ni and Ni/Au Schottky contacts of diameter 0.6 mm were resistively evaporated onto GaN through a metal mask at room temperature. To ensure temperature stability during deposition, the glass dome was cleaned of all metal residues before loading the samples for metallization. The thickness of the Au and Ni layers was 10 nm, and that of Ni/Au was 5/5 nm. Atomic Force Microscope (AFM) was used to study the morphology of Ni and Au onto GaN. Auger Electron Spectroscopy (AES) was used to characterize the Ni/Au layer after annealing in air for 5 minutes at 550 °C. Current voltage (*I-V*) measurements were taken using an HP4140B pA meter/DC source for all metal contacts.

6.4 Results and Discussion

Analysis of the metal films for continuity using AFM is presented in figure 6.2. The surface structure of all particles, even inside the etch pits, was found to be the same, indicating that the 10 nm metal film is continuous. Comparing Au and Ni, it is found that their surface structures on GaN differ. Ni films present smooth morphology and Au shows grained structures. The RMS roughness of the 10 nm Au and Ni are 25.6 and 22.7 nm respectively. Choosing an area without any etch pits, it was found that the peak-to-valley surface roughness of Ni films was approximately 9,0 Å and RMS roughness of 1.5 Å shows that the Ni films are relatively smooth. The Au peak to valley roughness was recorded as 11 nm and the RMS roughness 2.3 nm.



a) 10 nm Au layer



b) 10 nm Ni layer

Figure 6.2: The AFM images of 10 nm Au and Ni.

Figure 6.3 shows the Auger peak to peak heights (APPH) depth profiles as a function of sputtering time for as deposited (a) and annealed (b) at 500°C Au/Ni/GaN in air. The elements presented on the surface before anneal are Au, Ni, Ga, N and O as indicated. Figure 6.3(b) shows the formation of sandwiched layers after anneal. At highest APPH, we identify Au layer, presenting a compound as a result of annealing. The compound may be due to diffusion of elements during annealing. O and Ni compounds are also identified, followed by Ga and N compound. A diffused layer of Ni and Ga is seen at the beginning, showing a possible diffusion of Ni into GaN. At the end of sputtering, the depth profiles show that there exists a 1:1 ratio of Ni and O, indicating possible formation of NiO.

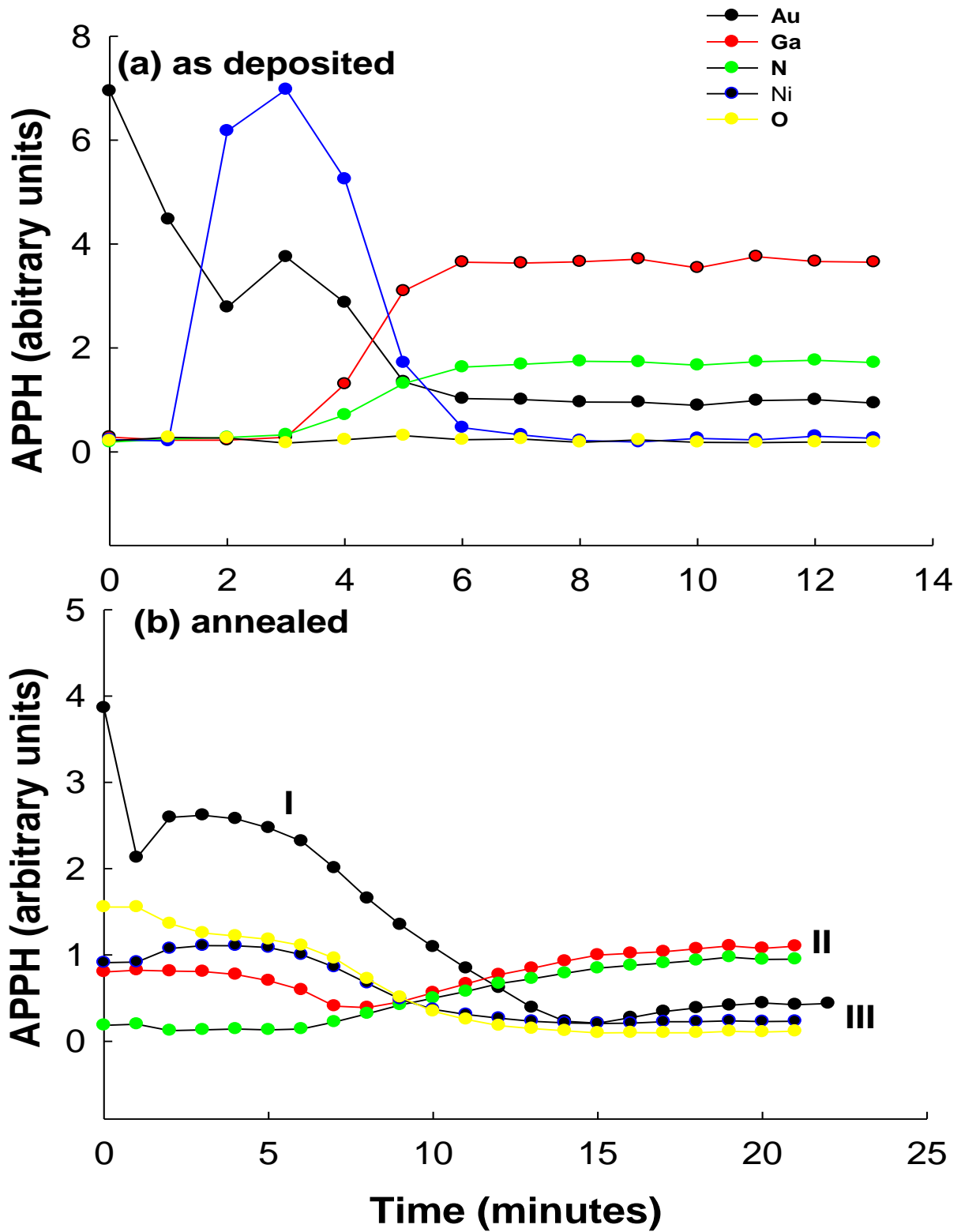


Figure 6.3: AES profiles of sputtered GaN/Ni/Au surface, (a) as deposited and (b) annealed.

Figure 6.4 is the RBS peak of Au, showing that Au has diffused into the Au/Ni/GaN structure during annealing so that we have a stack of compounds on GaN in agreement with AES results. In figure 6.3 (b), region I indicate the compound of Au, possibly with Ni as Au diffuses into the sample. A study of correlation of contact resistance with metal diffusion was done by Hu et. al. [9], using RBS. It was found that annealing Au/Ni/p-GaN for 10 minutes in air, Au diffused into the sample towards Ni and an out diffusion of Ni to the surface, resulting in the formation of NiO. Region II shows GaN compound and region III shows the formation of NiO.

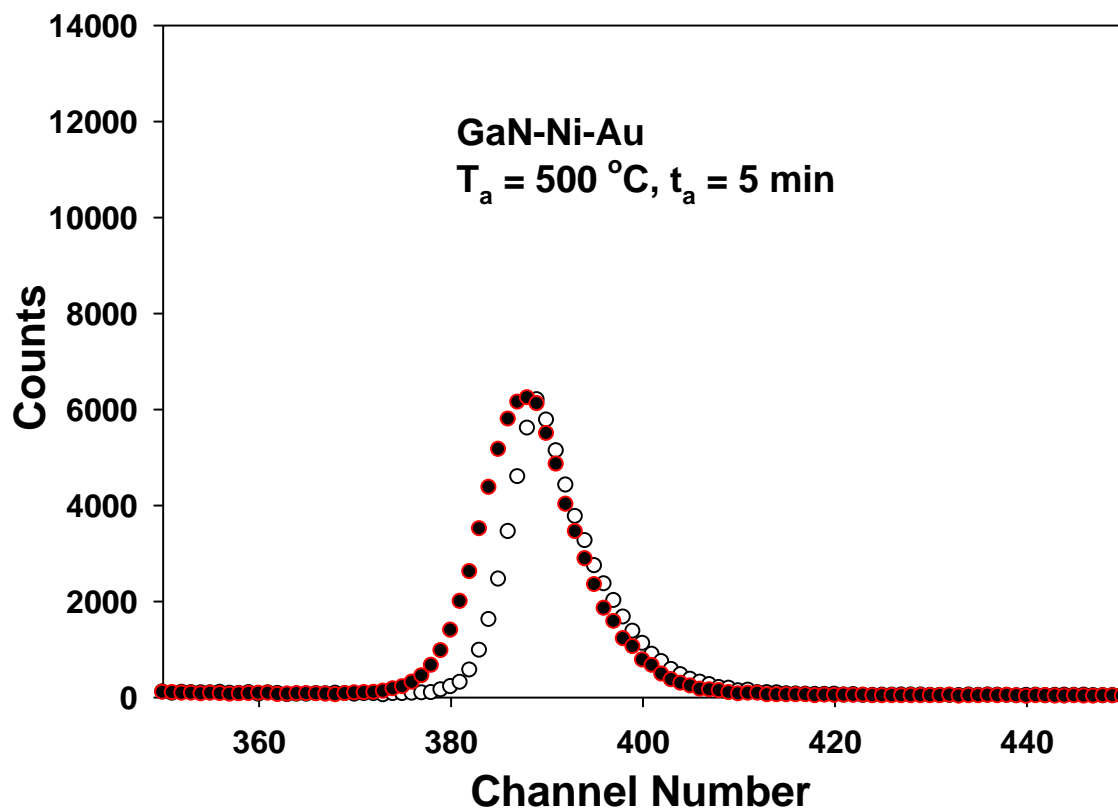


Figure 6.4: RBS spectra of Au profile, showing the as grown and annealed at 500 °C, where Au is seen to diffuse towards the interface.

A further study was done with 100 nm Ni onto GaN, annealed in air for one hour, to understand the compound formed at the Ni/GaN interface. In this study, XRD and SEM were used to analyse the samples. Figure 6.5 gives the XRD results indicating the formation of NiO and residual Ni onto GaN after 1 hour anneal. Electron Diffraction Spectroscopy (EDS) analysis of the annealed sample confirmed the observation, with ratio of Ni and O as almost 1:1. This is in agreement with work done by Nel et. Al., where it was shown that NiO formed at 500°C with no evidence of Ni₂O₃ phase [10].

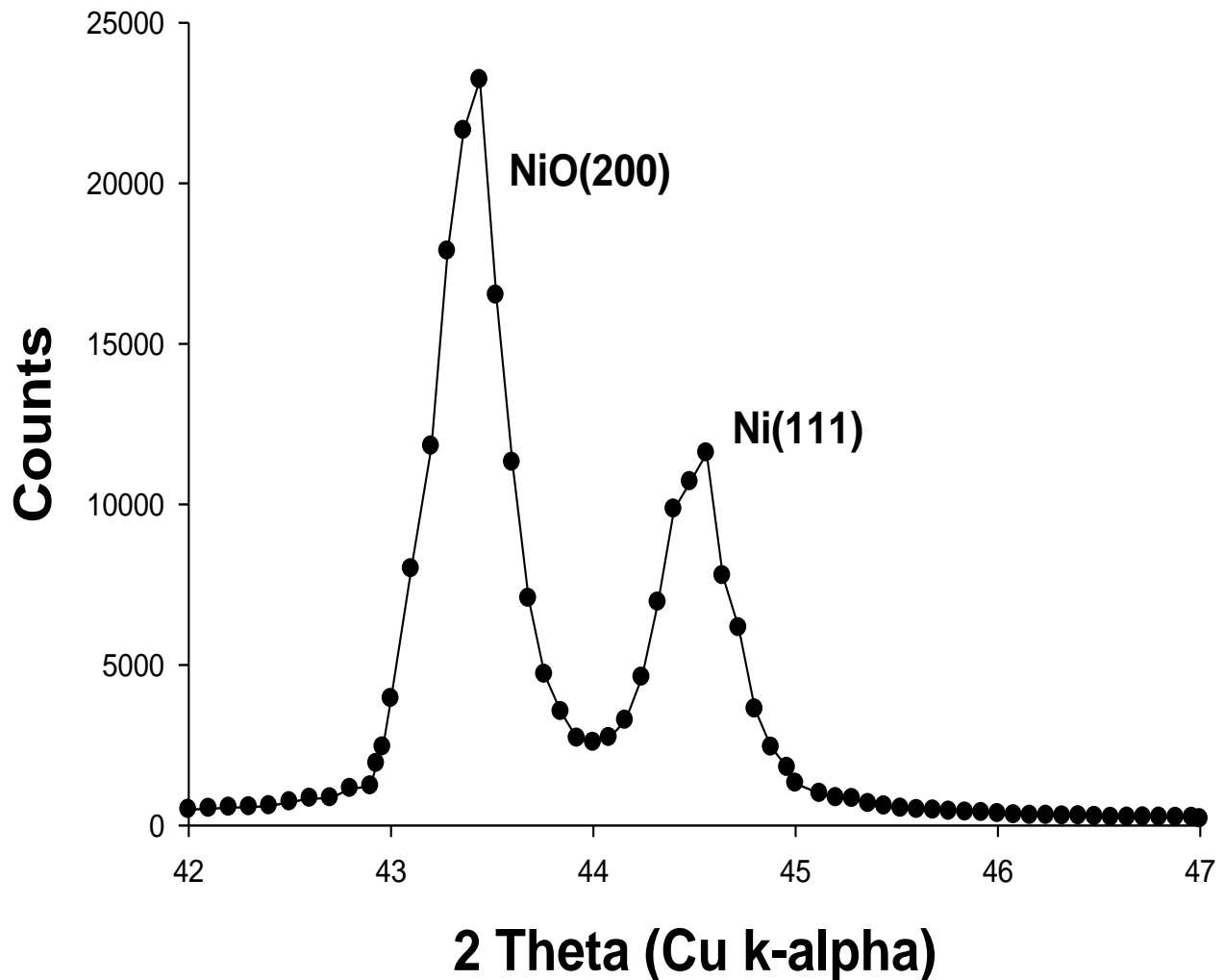


Figure 6.5: XRD patterns of oxidised Ni at 500°C showing the formation of NiO.

Figure 6.6 shows the current voltage mechanism of Au, Ni and Ni/Au contacts onto GaN. The Schottky barrier height of Au contacts was obtained as 0.81 ± 0.02 eV. Series resistance for these contacts was about $481 \pm 4 \Omega$. The current-transport mechanisms are dominated by thermionic emission at lower voltages and series resistance effect depicted clearly at higher voltages. Generally Au contacts age very quick due to the problem of adhesion to GaN. The Schottky barrier height of Ni contacts was obtained as 0.78 ± 0.04 eV Series resistance for these contacts was about $38 \pm 1 \Omega$, far less than that of Au contacts. Ni/Au contacts are annealed at 500°C for transparency. The leakage current of Ni/Au is two orders of magnitude lower than that of Ni, and the Schottky barrier height was averaged at 0.92 ± 0.01 eV. Current transport mechanisms are clearly displayed with generation-recombination dominating the lower voltage region. In the high voltage region, the diode characteristics are affected by series resistance. The presence of NiO onto GaN reduced the leakage current by two orders of magnitude.

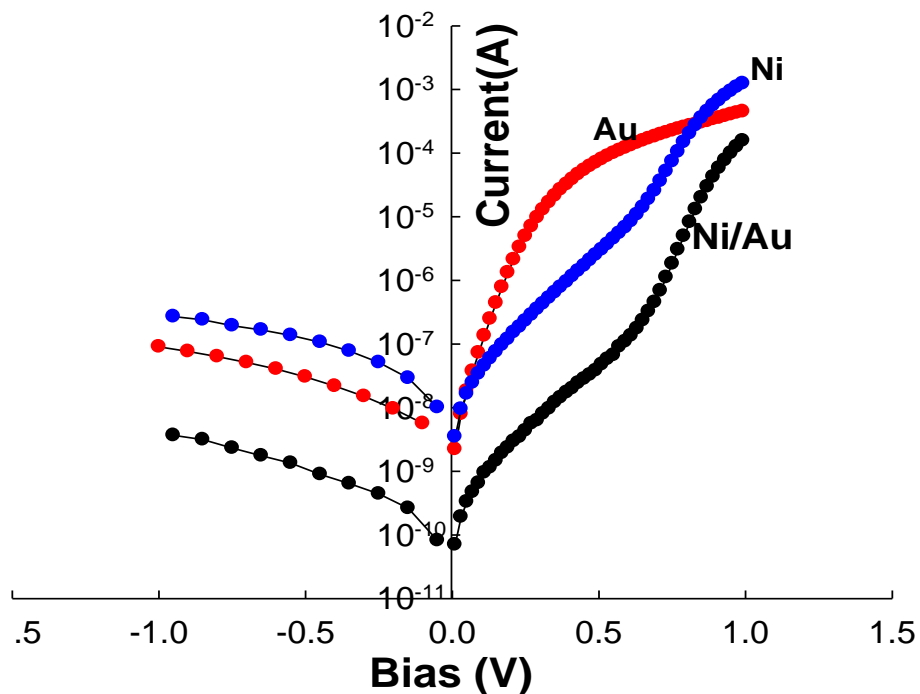


Figure 6.6: Current-Voltage plots of Au, Ni and Ni/Au contact on n-GaN. Ni/Au was annealed at 500°C while Ni and Au are 10 nm each thick and are not annealed.

6.5 Conclusions

In conclusion, Au, Ni and Ni/Au contacts onto GaN were fabricated and characterized. AFM showed that 10 nm thick Au and Ni contacts onto GaN were continuous with peak-to-valley surface roughness of Ni films approximately 9.0 Å and RMS roughness of 1.5 Å while Au peak to valley roughness was recorded as 11 nm and the RMS roughness 2.3 nm. Annealing Ni/Au onto GaN produced a highly transparent and conductive NiO, as confirmed by XRD, SEM, AES sputtering profiles and EDS analysis. *I-V* characteristics showed that Ni/Au contacts had the lowest reverse leakage current, two orders of magnitude below that of Au contacts. The barrier heights of the diodes were 0.81, 0.78 and 0.92 for Au, Ni and Ni/Au respectively.

REFERENCES

- [1] Monroy E., Calle F., Munoz E., Omnes F., Gibart P. and Munoz J. A., Applied Physics Letters **73** (1998) 2146.
- [2] Osinsky A., Gangopadhyay V, Lim B. W., Anwar A. Z., Asif-Khan M., Kuksenkov D. V. and Temkin H., Applied Physics Letters **72** (1998) 742.
- [3] Luther B. P, Wolter S. D. and Mahoney S. E., Sensors and Actuators B, **56** (1999) 164.
- [4] Sheu L. K., Su Y. K., Chi G. C., Koh P. L., Jou M. J., Chang C. M., Liu C. C. and Hung W. C., Applied Physics Letters **74** (1999) 2340.
- [5] Sawatzky G. A and Allen J. W., Physical Review Letters **53** (1984) 2339.
- [6] Liday J., Hotovy I., Sitter H., Vogrincic P., Vincze A, Vavra I, Satka A., Ecke G., Bonnani A., Breza J., Simbrunner C. and Plchberger B., Journal Materials Science **19** (2008) 855.
- [7] Auret F. D., Wu L., Meyer W. E., Nel J. M., Legodi M. J. and Hayes M., Physica Status Solidi (c) **1** (2004) 674.
- [8] Su Y. K, Chang S. J, Chen C. H, Chen J. F., Chi G. C, Sheu J. K., Lai W. C. and Tsai J. M., IEE Sensors Journal **2** (2002) 7361
- [9] Hu C. Y., Ding Z. B., Qin Z. X., Chen Z. Z., Yang Z. J., Yu T. J., Hu X. D., Yao S. D. and Zhang G. Y., Semiconductor Science and Technology **21** (2006) 1261.
- [10] Nel J. M., Auret F. D., Wu L., Legodi M. J. and Hayes M., Sensors and Actuators B: Chemical **100** (2004) 270.

CHAPTER 7

Chemical treatment effect on Au/GaN diodes

7.1 Introduction

Rectifying contacts with low leakage currents and high barrier height are required for the successful fabrication of GaN-based devices. Schottky barrier diodes (SBD) are the choice structure for many semiconductor devices, including microwave diodes, field-effect transistors and photodiodes [1,2,3]. Their technological importance requires a full understanding of the nature of the electrical characteristics of SBDs. It is well known that SBD has a thin layer of an oxide between the metal and the semiconductor, which cannot be removed by conventional chemical cleaning. Such an oxide converts the diode to metal-insulator-semiconductor (MIS) and usually influences the electrical characteristics of the diode, causing a change in the interfacial charge with bias, giving rise to an electric field at the interfacial layer between the metal and the semiconductor [4,5]. The oxide layer reduces the barrier height and consequently increases the series resistance.

Generally, the forward biased current-voltage (I-V) characteristics are linear in the semi-logarithmic scale at low voltages, but deviate considerably from linearity due to the effects of series resistance, R_s , resulting from the presence of the thin oxide layer and other surface contaminants. The series resistance is only effective in the curvature downward region or non-linear region of the forward I-V characteristics at sufficiently high voltages. The concavity of the current-voltage characteristics at higher voltages increases with increasing series resistance. Increasing series resistance decreases the barrier height and this result in non-ideal current-voltage characteristics. Other parameters such as the ideality factor, $n(V)$ and zero biases-barrier height, $\Phi_{b,0}$ are effective in both the linear and the non-linear regions of the I-V curve, accompanying the changes in the Schottky barrier height (SBH) [6]. The effect of the series resistance between the depletion region and the ohmic contact of the neutral region of the

semiconductor bulk causes the I-V characteristics of the metal-semiconductor contact to deviate from the expected [7].

The interface states at the metal-semiconductor junction play a vital role in evaluating the Schottky barrier height and the ideality factor. These manifest themselves as deviations from the ideal Schottky barrier formation and are localized within a few atomic layers of the intimate metal-semiconductor contact with energies which fall inside the forbidden gap. Bardeen showed that such charge accumulated at the metal-semiconductor contact reduces the effective potential difference between the semiconductor and the metal contact [8]. Interface states arise from semiconductor surface states due to discontinuity in the lattice potential, metal-induced-gap states due to wave-function tunneling from the metal into the semiconductor, surface states due to contamination and defects; and any new compounds formed as a result of the interaction of the metal and the semiconductor.

A study of the importance of series resistance in calculating the characteristics parameters of Si Schottky contacts was done by Aydin et al [7], obtaining their estimations from determination of interface states density distribution from the analysis of the current voltage measurements. Kampen and Monch studied the barrier heights of different metals on GaN using metal-induced gap states (MIGS) and the electronegativity model, concluding that the experimental values of the barrier height are excellently reproduced by the theoretical predictions, which follow from physical MIGS and the electronegativity concept [9]. A review of metal-contact technology has revealed the importance of surface preparation prior to metal deposition [10]. In this study, two different surface chemicals were used to treat GaN surface prior to metal deposition. The effects of chemical treatments on Schottky characteristics were investigated using capacitance-voltage (*C-V*) and current-voltage (*I-V*) characteristics. The average barrier height for the diodes was 1.43 and 1.20 eV for *C-V*; and 0.81 and 0.89 for *I-V* measurements respectively.

7.2 Experimental.

For this investigation, we have used GaN samples with carrier density of $1 \times 10^{17} \text{ cm}^{-3}$, obtained from TDI. Before contact fabrication, samples were cleaned using trichloroethylene (TEC), Isopropanol and HCl:HNO₃ aquaregia. Each of the samples was finally etched in 1:1 HCl:H₂O (sample 1) and (NH₄)₂S (sample 2) respectively. Using patterned surface, Ti/Al/Ni/Au (150/2200/400/500 Å) ohmic contacts were deposited by electron-beam and annealed in ultra pure Ar for 5 minutes at 500 °C. Thereafter, Au Schottky contacts, 0.25 mm thick, were deposited in the resistive evaporator at room temperature. The values of zero-biased barrier height and ideality factor were determined from *I-V* and *C-V* measurements at room temperature and corrected afterwards for the effect of series resistance.

7.3 Results and Discussion

7.3.1 Capacitance-Voltage

In Schottky diodes, the depletion layer capacitance can be expressed as [1]

$$C^{-2} = \frac{2(V_{bi} - V_A)}{q\epsilon_s A^2 N_D} \quad (1)$$

where A is the area of the diode, V_{bi} the diffusion potential at zero bias and is determined from the extrapolation of the linear $C^{-2} - V$ plot to the V axis, and V_A is the applied voltage. The value of the barrier height can be obtained from the relation:

$$\Phi_{b,0}(C - V) = V_{bi} + V_0 \quad (2)$$

where V_0 is the potential difference between the bottom of the conduction band and the Fermi level; and can be calculated knowing the donor concentration N_D obtained from the following relation:

$$(3)$$

where $N_C = 4.6 \times 10^{16} \text{ cm}^{-3}$ is the effective density of states in the conduction band [2].

Nine dots with the same diameter (0.25 mm) on each sample were evaluated. Figure 7.1 shows the reverse bias $C^{-2} - V$ characteristics for one diode from sample 1 and sample 2 respectively. For these particular diodes on samples 1 and 2, the C-V barrier heights are 1.43 and 1.20 eV respectively. The carrier concentration of 1.9×10^{16} and $2.4 \times 10^{16} \text{ cm}^{-3}$ from the reverse bias $C^{-2} - V$ plots were obtained for sample 1 and sample 2. The C-V barrier heights ranged from 1.28 to 1.50 eV for sample 1 and from 1.14 to 1.25 eV for sample 2. The statistical analysis for the C-V data yielded SBH mean value of 1.35 ± 0.04 eV for t sample 1 dots and SBH mean value of 1.20 ± 0.03 eV for sample 2.

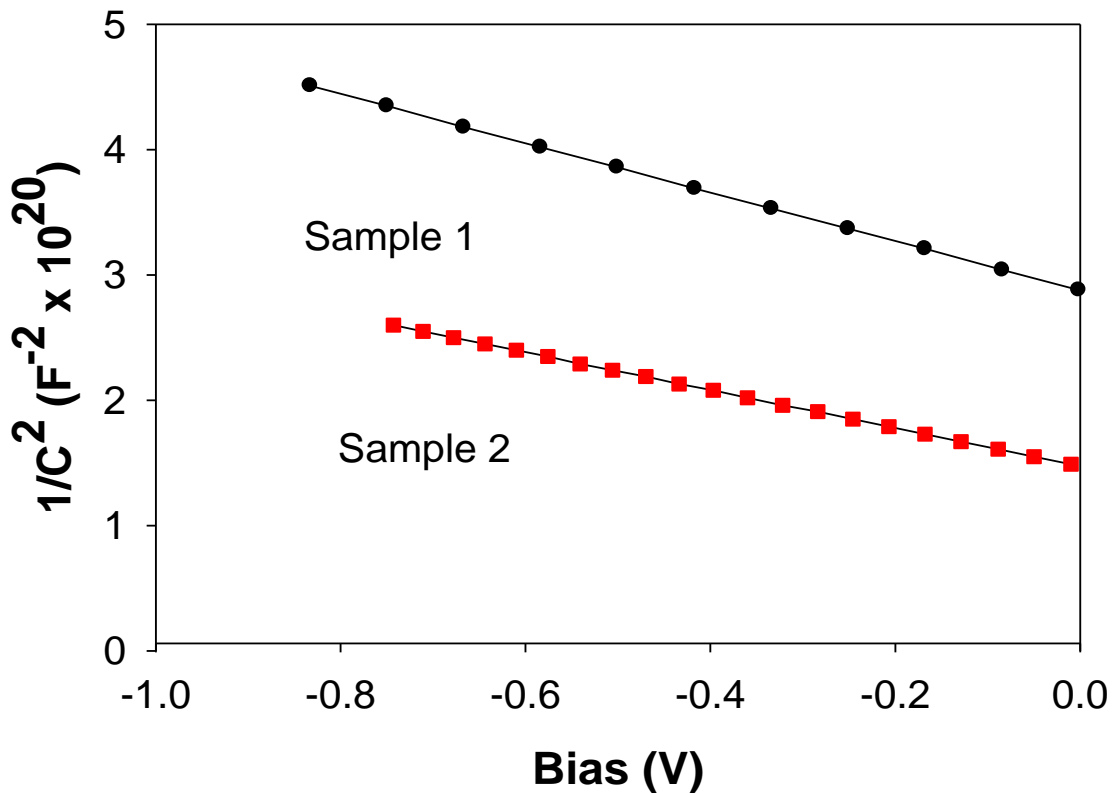


Figure 7.1: Reverse Bias $C^2 - V$ curves of the HCl and $(\text{NH}_4)_2\text{S}$ samples. For these particular diodes on samples 1 and 2, the C-V barrier heights are 1.43 and 1.20 eV respectively.

7.3.2 Current-Voltage

In Schottky barrier diodes, the barrier height depends on the voltage and surface conditions prior to metal deposition. The surface condition includes the thickness of the interfacial oxide, which affects the current-transport mechanisms. These include the thermionic emission, which is characterized by ideality close to unity and thermionic field emission and field emission. These mechanisms are affected by series resistance, tunneling and generation recombination in the depletion region. Table 1 gives the summary of the electrical characteristics of the diodes.

Table 7.1: Values obtained experimentally from the current-voltage characteristics of the Au/GaN Schottky diodes. The difference in series resistance for the sample 1 and 2 is due to the surface state after different chemical treatment.

Sample 1	n	1.17
	$R_s (\Omega)$	22.3
	$\Phi_{b,c}$ (eV), C-V	1.43
	$\Phi_{b,0}$ (eV), I-V	0.82
Sample 2	n	1.89
	$R_s (\Omega)$	17.1
	$\Phi_{b,c}$ (eV), C-V	1.20
	$\Phi_{b,0}$ (eV), I-V	0.71

For a Schottky contact with series resistance, the net current of the device is due to thermionic emission and it is written as [1]:

$$I = I_0 \exp\left(-\frac{q(V_A - IR_s)}{nkT}\right) \quad (4)$$

where the saturation current I_0 is expressed as

$$I_0 = AA^*T^2 \exp\left(-\frac{q\Phi_{b,0}}{kT}\right) \quad (5)$$

where q is the electron charge, A^* is the effective Richardson constant and is equal to $26A/cm^2K^2$ for n-type GaN [11], A is the diode area, T is the absolute temperature, k Boltzmann

constant, n the ideality factor of the SBD and $\Phi_{b,0}$ the zero bias barrier height. When $V_A \geq 3kT/q$, the extrapolated current, I_0 , and the zero bias barrier height can be expressed as

$$\Phi_{b,0} = \frac{kT}{q} \ln \left(\frac{A^* AT^2}{I_0} \right) \quad (6)$$

and the ideality factor from equation 4 can be written as

$$n = \frac{q}{kT} \frac{dV}{d \ln I} \quad (7)$$

The ideality factor of the SBD, n is a measure of the conformity of the diode to pure thermionic emission. From figure 7.2, current-transport mechanisms displayed are thermionic emission and the series resistance effect at high voltages. The values of the ideality factor, n , and the barrier height Φ_b were calculated from the forward I - V characteristics according to (6) and (7). For sample 1 the barrier height, $\Phi_{b,0}$ ranged from 0.79 to 0.89 eV and the ideality factor n ranged from 1.02 to 1.17. Sample 2 $\Phi_{b,0}$ values ranged from 0.71 to 0.85 eV and the n from 1.31 to 1.36. The statistical analysis yielded mean values of 0.84 ± 0.05 eV for the 1.06 ± 0.50 for barrier height and ideality factor of sample 1 (9 dots) respectively and the mean values of 0.80 ± 0.01 eV and 1.34 ± 0.20 (9 dots) for sample 2 diodes. Ideality factors above unity has been attributed to: interface states due to thin oxide layer between the metal and the semiconductor, including other contaminants, tunneling currents in highly doped semiconductors, image-force lowering of the Schottky barrier in electric field at the interface, and generation-recombination currents within the depletion region [1]. Our previous results have shown S and Cl residues onto GaN after cleaning in HCl and $(\text{NH}_4)_2\text{S}$ using Auger Electron Spectroscopy (AES) and X-ray Photoemission Spectroscopy (XPS) [12]. The work done on GaAs and GaP nitridation has shown anion exchange where a thin layer of Ga-N was formed on each of the materials [13]. Surface Ga-N in turn passivates the GaAs and GaP, affecting the I-V and C-V characteristics of these materials. In addition, the work done by Liu et al has shown that the Ga peak becomes larger when samples are cleaned in $(\text{NH}_4)_2\text{S}$ than in HF/HCl [14]. Furthermore, $(\text{NH}_4)_2\text{S}$ has been found to reduce the barrier height on GaN, and preventing re-oxidation of the surface [15]. We suggest that there exist Ga-Cl and Ga-S on sample 1 and sample 2, respectively. Previous

XPS results have shown that as-grown GaN surface has oxides in the form of Ga_2O_3 and GaOH [12]. In addition, while rinsing GaN in water, addition of OH to GaN to form the GaOH , may occur, and be part of sticking surface water that may contribute to interface states [16].

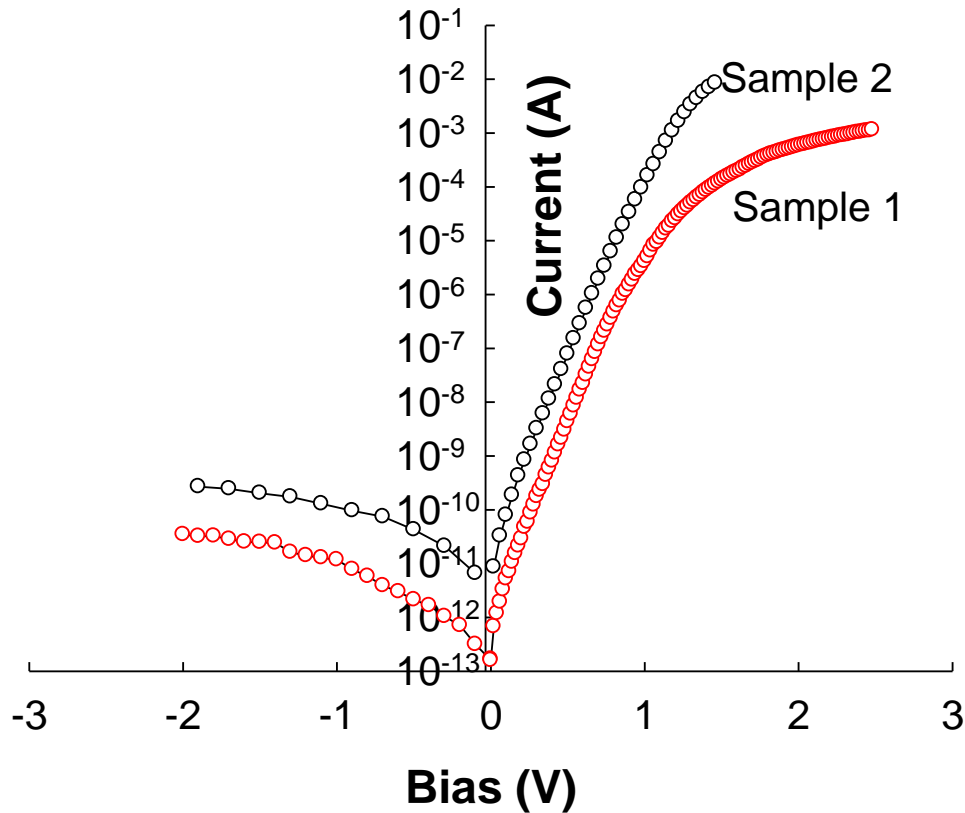


Figure 7.2: *I-V* curves of the treated samples. The series resistance values of HCl samples are generally higher than those treated in $(\text{NH}_4)_2\text{S}$, which presented less oxide and reduced barrier height

The values of R_s and $\Phi_{b,0}$ for both sample 1 and 2 were obtained as 0.82 eV and 22.3 Ω ; and 0.71 eV and 17.0 Ω respectively. As mentioned above, the barrier height values of 1.43 and 1.20 eV for sample 1 and 2 were obtained from the C^{-2} - V plots, respectively. These barrier height values obtained from the C^{-2} - V (1.43 eV) and *I-V* characteristics (0.89 eV) are different from each other by 0.54 eV. We attribute the difference between the *I-V* and *C-V* barrier height in the metal-semiconductor to SBH inhomogeneity. This is the fact that the barrier heights of the

diodes on the same sample differs from diode to diode and at different positions on the same diode. The measured I - V barrier height is significantly lower than the weighted arithmetic average of the SBHs. On the other hand, the C - V measured barrier height is influenced by the distribution of charge at the depletion region follows the weighted arithmetic average of the barrier height inhomogeneity; hence the BH determined by C - V is close to the weighted arithmetic average of the barrier heights. Therefore, the barrier height determined from zero bias intercept assuming thermionic emission as current transport mechanism is well below the measured BH and the weighted arithmetic average of the barrier heights [17,18]. Furthermore, the surface damage at the metal-semiconductor-interface affects the I - V measurements because defects may act as recombination centers for trap-assisted tunneling currents. C - V measurements are generally less prone to interface states, so that the determined barrier height is considered more reliable, though the depletion width can be altered by the interface defects if they are deeper into the space charge region [19].

7.4 Conclusions

In conclusion, we have fabricated Au/n-GaN SBDs using different cleaning procedures. From the current-voltage characteristics, we obtained the values of ideality factor, SBH, and R_s for the samples. I - V characteristics are near ideal with thermionic emission as the dominant current transport mechanism. Furthermore, HCl treated samples behave like a MIS diode due to the amount of oxide remaining on the surface after treatment. The series resistance values of HCl samples are generally higher than those treated in $(\text{NH}_4)_2\text{S}$, which presented less oxide and reduced barrier height, in agreement with published results. Most published results on GaN have only reported their findings without specifics on current transport mechanism. Thus further work is needed for the investigation ideality factor far above unity, which will need the knowledge of the oxide layer thickness on GaN, effects of passivation of GaN surface on electrical characteristics, and analysis of barrier height inhomogeneities on the rectifying diode characteristics on GaN.

REFERENCES

- [1] Rhoderick E. H. and Williams R. H., Metal-Semiconductor Contacts, Oxford, Clarendon, (1988).
- [2] Sze S. M., Physics of Semiconductor Devices, 2nd Edition, New York, Wiley (1981).
- [3] Wang L., Nathan M. I., Lim T-H, Asif Khan M. and Chen Q, Applied Physics Letters **68** (1996) 1267.
- [4] Hanselaer P., Laflere W.H., Meirhaeghe R. L. and Cardon F., Applied Physics Letters **56** (1984) 2309.
- [5] Monroy E., Calle F., Pau J.L., Muñoz E. and Omnes F., Electronic Letters **36** (2000) 2096.
- [6] Card J. C. and Rhoderick E. H., Journal of Applied Physics: D **4** (1971) 1589.
- [7] Aydin M. E., Akkiliç K. and Kiliçoğlu T., Applied Surface Science **225** (2004)1304.
- [8] Bardeen J., Physical Review, **71** (1947) 771.
- [9] Kampen T. U. and Monch W., Applied Surface Science 117/118 (1997) 388.
- [10] Liu Q. Z. and Lau S . S., Solid State Electronic **42** (1998) 677.
- [11] Schmidt A. C., Ping A. T., Asif Khan M., Chen Q., Yang J. W. and Adesida I., Semiconductor Science and Technology, **11** (1996) 1464.
- [12] Diale M., Auret F. D., Van der Berg N. G., Odendaal R. Q. and Roos W. D., Applied Surface Science **246** (2005) 279.
- [13] Bruno G., Applied Surface Science **235** (2004) 239.
- [14] Liu J., Shen B., Zhou Y. G., Zhou H. M., Wang M. J., Zheng Z. W, Zhang B., Shi Y. and Zheng Y. D., Optical Materials **23** (2003) 133
- [15] Cao X. A., Pearton S. J., Dang G., Zhang A. P., Ren F. and Van Hove J. M., Applied Physics Letters,**75** (1999) 4130.
- [16] Diale M., Auret F. D., Van der Berg N. G., Odendaal R. Q. and Roos W. D., Surface and Interface Analysis **37** (2005) 1158.
- [17] Werner J. H. and. Guttler H. H, Journal of Applied Physics, **69** (3) (1991) 1552.
- [18] Tung R. T., Levi A. F. J., Sullivan J. P. and Schrey F., Physical Review Letters **66** (1971) 72.
- [19] Fontaine C., Okumura T. and Tu K. N., Journal of Applied Physics **54** (1983) 1404.

CHAPTER 8

Fabrication and characterization of GaN and AlGaN Schottky barrier photodiodes

8.1 Introduction

GaN is a wide bandgap semiconductor that has been explored for the fabrication of ultraviolet photodiodes suitable for operations in chemically harsh and high temperature environments [1]. Alloying of Al with GaN to form AlGaN has a very important property called solar-blindness, which makes the material insensitive to visible light [2]. Intrinsic solar-blindness is a bandgap dependent property of the semiconductors [3]. The bandgap of GaN and AlN are 3.4 and 6.2 eV respectively, which makes AlGaN bandgap to lie between the two extremes for the specified Al content. [4]. Similar to GaN, the growth of AlGaN had issues such as lack of suitable substrate, resulting in cracks in the thin film [5]. AlGaN grown on sapphire has high densities of threading dislocation which increases with increasing Al content [6]. Threading dislocations are detrimental to devices as they are a major reason for high leakage currents and reduced spectral responsivity in semiconductor photodiodes [7]. There has been much progress in the growth of AlGaN, with the use of AlN nucleation layer to reduce cracks in the AlGaN film [8].

Schottky barrier photodiodes are used in applications such as missile warning and guidance, flame monitoring and prevention of skin cancer [9]. Thus far, various types of GaN-based photodetectors have been reported, with low dark current, high response speed, and high detectivity [10]. They have reported low capacitance, which is an important component of large bandwidth and low noise performance in photodetectors. Another important parameter is high transparency of the metal used for Schottky barriers, which determines the number of photons entering the semiconductor [11]. In this work, we have fabricated GaN and AlGaN Schottky barrier photodiodes, using Ni/Au metallization system. The photodiodes were characterized in our in-house electro-optical measurement station. The photodiodes gave zero biased dark

currents as small as 10^{-9} A ($35.8 \mu\text{A}/\text{cm}^2$) for GaN and 2.8×10^{-9} A ($21.6 \text{nA}/\text{cm}^2$) for AlGaN (55% Al). The recorded reverse biased peak responsivity was 31.8 A/W with quantum efficiency of 11 % when the wavelength of light is 369 nm in the case of GaN. AlGaN results have shown a peak responsivity of 3.8 mA/W at 280 nm, with quantum efficiency of 1.7 %.

8.2 Experimental

GaN samples used in the experiment were $5.6 \mu\text{m}$ thick, grown by HVPE. AlGaN epitaxial structures were grown by HVPE with 55 % Al content. This structure consist of 30 nm GaN grown on sapphire followed by Si doped GaN film for the fabrication of ohmic contacts. The following layer was $0.1 \mu\text{m}$ AlN, which is believed to reduce threading dislocations in AlGaN film. The active layer was a thin film of $0.5 \mu\text{m}$ layer of $\text{Al}_{0.55}\text{Ga}_{0.45}\text{N}$. Samples were cleaned in organic solvents, boiled in HCl:HNO₃ aquaregia and a final etch in HCl, prior to loading in the electron-beam deposition system for ohmic contacts consisting of Ti/Al/Ni/Au onto the top layer. All rinsing was done in methanol. The ohmic contacts were then annealed in Ar ambient for 5 minutes at $500 \text{ }^\circ\text{C}$.

The samples were then etched in HCl before loaded for the deposition of Schottky contacts in the resistive evaporator, consisting of Ni/Au with thickness 5 nm each. Similarly, GaN photodiodes were fabricated, using the same cleaning procedure and the same metals as with AlGaN for both ohmic and Schottky contacts. For device characterization, current-voltage (*I-V*) measurements were carried out. *I-V* measurements were taken using an HP4140B pA meter/DC source. Dark- and photocurrent were measured from annealed samples. Wavelength dependent measurements were done at the same *I-V* station with a deuterium lamp connected to the monochromator by optical fibre. All measurements were performed at room temperature. Using the commercial SiC and AlGaN photodiodes' data sheets and the quantum efficiencies specified therein, the irradiance was determined, which was then used to calculate the responsivities and quantum efficiencies of the fabricated diodes.

8.3 Results and Discussion

The GaN photodiodes have recorded a zero biased dark current as low as 6.48×10^{-9} A ($35.8 \mu\text{A}/\text{cm}^2$) while that of AlGaN was 2.8×10^{-9} A ($21.6 \mu\text{A}/\text{cm}^2$). Figure 8.1 (a) and (b) shows the I-V characteristics of GaN and AlGaN photodiodes respectively. The barrier height of 0.67 eV was recorded for *I-V* measurements and the corresponding ideality factor of 2.48. The series resistance of the diodes was 381 Ω . In the case AlGaN the *I-V* barrier height was 1.09. The ideality factor for Schottky diodes fabricated on AlGaN was 1.35 with series resistance in 1090 Ω . Schottky diodes on GaN and AlGaN suffer from high series resistance. Series resistance in AlGaN/GaN structures increases with increasing Al content and thickness of thin film. High series resistance contributes to slow response and thermal noise of the photodiodes.

Schottky barrier GaN photodiodes with dark currents densities as low as 10^{-10} A/cm² have been reported [12]. The reported low current densities were measured at higher voltages of up to 50 V when device active areas were differing from one device to the other. From the work done by Zhou et al [13], in annealing the Ni/Au contacts in oxygen, low dark currents were observed. Our Ni/Au contacts were annealed in air. Su et al [14], have compared GaN and AlGaN photodetectors, where high quantum efficiencies and low noise levels in AlGaN were reported. The fact that the ideality factors of the diodes are all far above unity, indicates that the total current is a combination of current mechanisms, other than thermionic emission [15]. The low values of barrier height show that we have fabricated GaN photodiodes which allows majority carriers to easily cross from the metal to the semiconductor. Consequently, such diodes have long cut-off wavelength, so that GaN-Ni/Au pair are correctly selected for UV detection. The dark current can be further lowered by cooling the photodiodes.

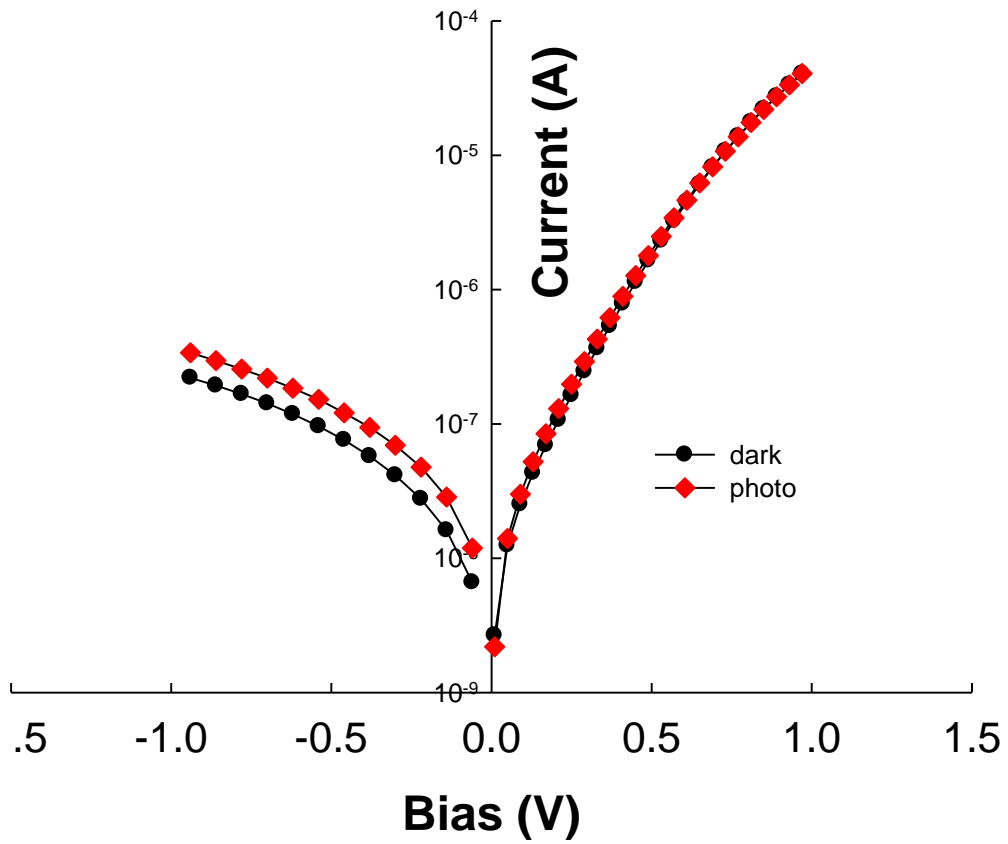


Figure 8.1 (a): *I-V* characteristics of GaN photodiodes.

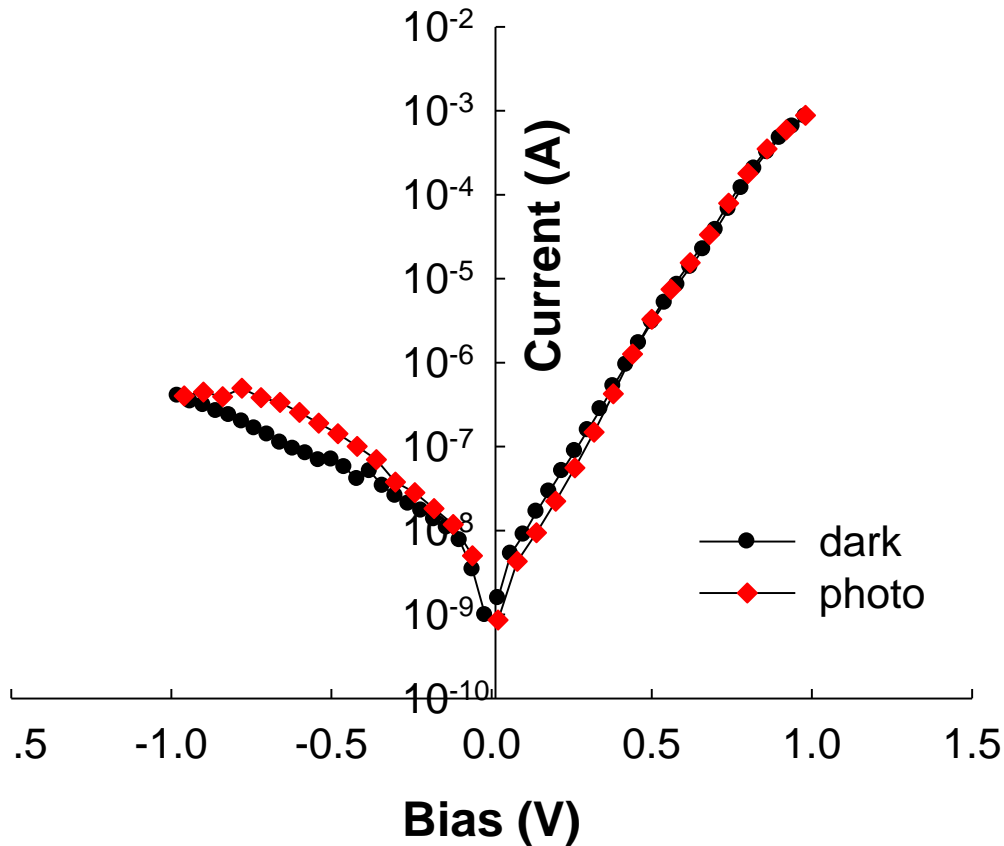


Figure 8.1 (b): *I-V* characteristics of AlGaN photodiodes.

Spectral responsivity measurements were done in the 150–450 nm range, using Deuterium lamp, a single-pass monochromator and a calibrated SiC or AlGaN photodetector. The response curves of commercial AlGaN and laboratory AlGaN are presented in figure 8.2, confirming the optoelectronic station accuracy. The peak responsivity of the commercial AlGaN photodiode occurred at 45.8 at 270 nm, with 21 % quantum efficiency. During the measurements, applied voltage on the photodetector was varied from 0.1 – 0.5 V. The responsivity of a photodiode is a measure of the effectiveness of the conversion of incident radiation into current or voltage and can be expressed as [16]:

$$R_{\lambda} = \frac{I_p}{P_{opt}} = \frac{\eta q}{h\nu} = \frac{\eta \lambda}{1.24} \frac{\mu m}{AW^{-1}} \quad (1)$$

where $I_p, P_{opt}, \eta, q, h, \nu$ and λ are the photocurrent, optical power, quantum efficiency, electron charge, Plank's constant, frequency and wavelength respectively. The irradiance of the lamp was estimated from the factory settings of the detector; using the calibration values to evaluate the optical power. Using equation (1) the peak responsivity, R_λ of 31.8 mA/W was recorded for GaN and 3.8 mA/W for AlGaIn respectively. The maximum photo response occurred at 369 nm and 280 nm wavelengths for GaN and AlGaIn photodiodes, as shown in Figure 8.3 (a) and (b) respectively. Since $\lambda_c < 280$ nm was satisfied, true solar-blind detection was successfully demonstrated for AlGaIn photodiodes, while GaN satisfied the condition for visible-blind photodiodes at $\lambda_c < 380$ nm [17]. The quantum efficiency (Q.E), defined as the percentage of incident photons that contribute to the photocurrent, follows from equation (1) and is given by:

$$\eta = \frac{R_{observed}}{R_{ideal}(100\%)} = R_\lambda \frac{hc}{q} = 1240 \frac{R_\lambda}{\lambda(nm)} \quad (2)$$

Maximum quantum efficiency of GaN and AlGaIn photodetector determined from the responsivity value was about 11 % and 1.7% respectively. The low Q.E of AlGaIn photodiodes shows that very little light was absorbed.

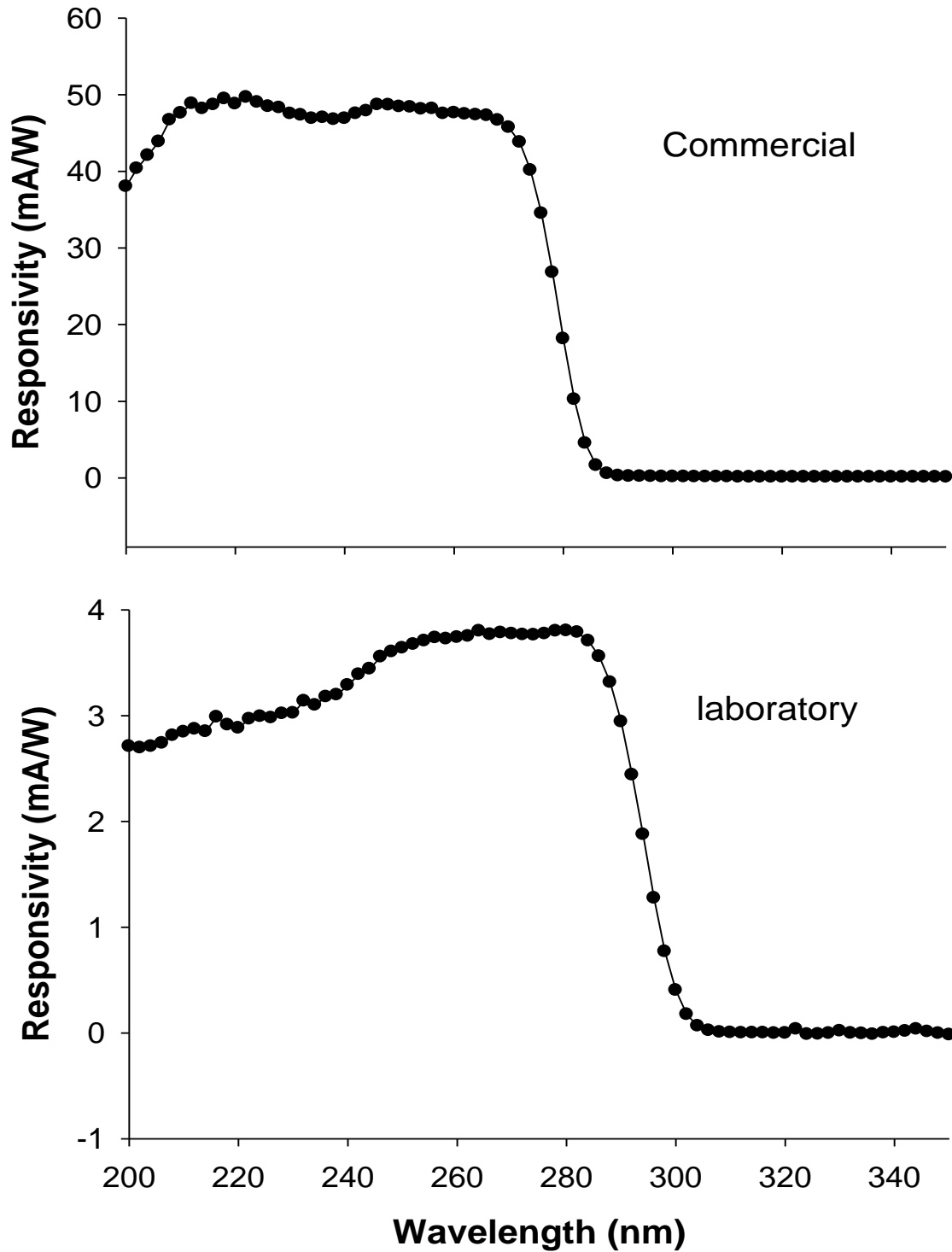


Figure 8.2: Photocurrent density response curves as a function of wavelength for AlGaN UV detectors.

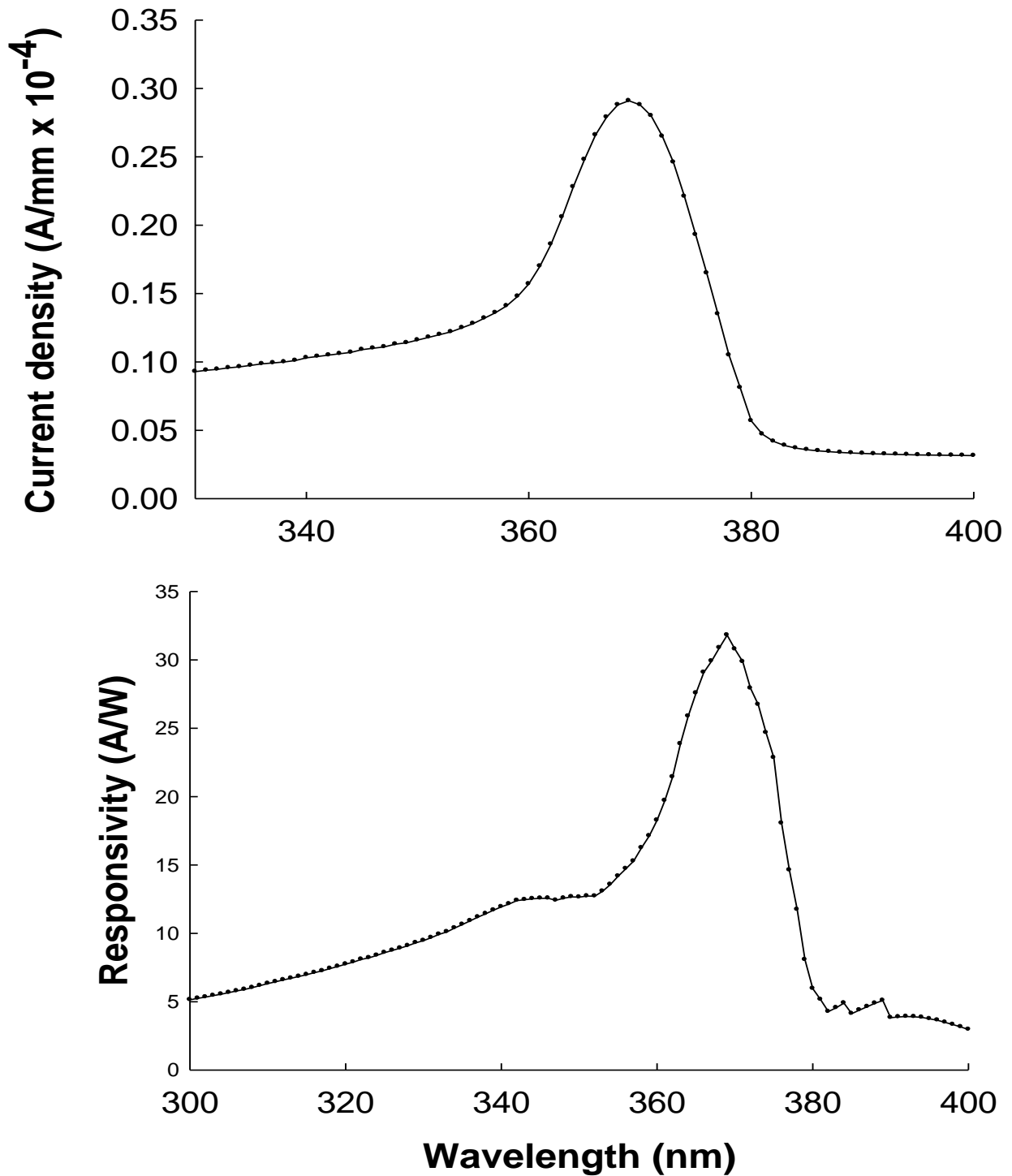


Figure 8.3 (a): Photocurrent density response curves as a function of wavelength for GaN UV detectors

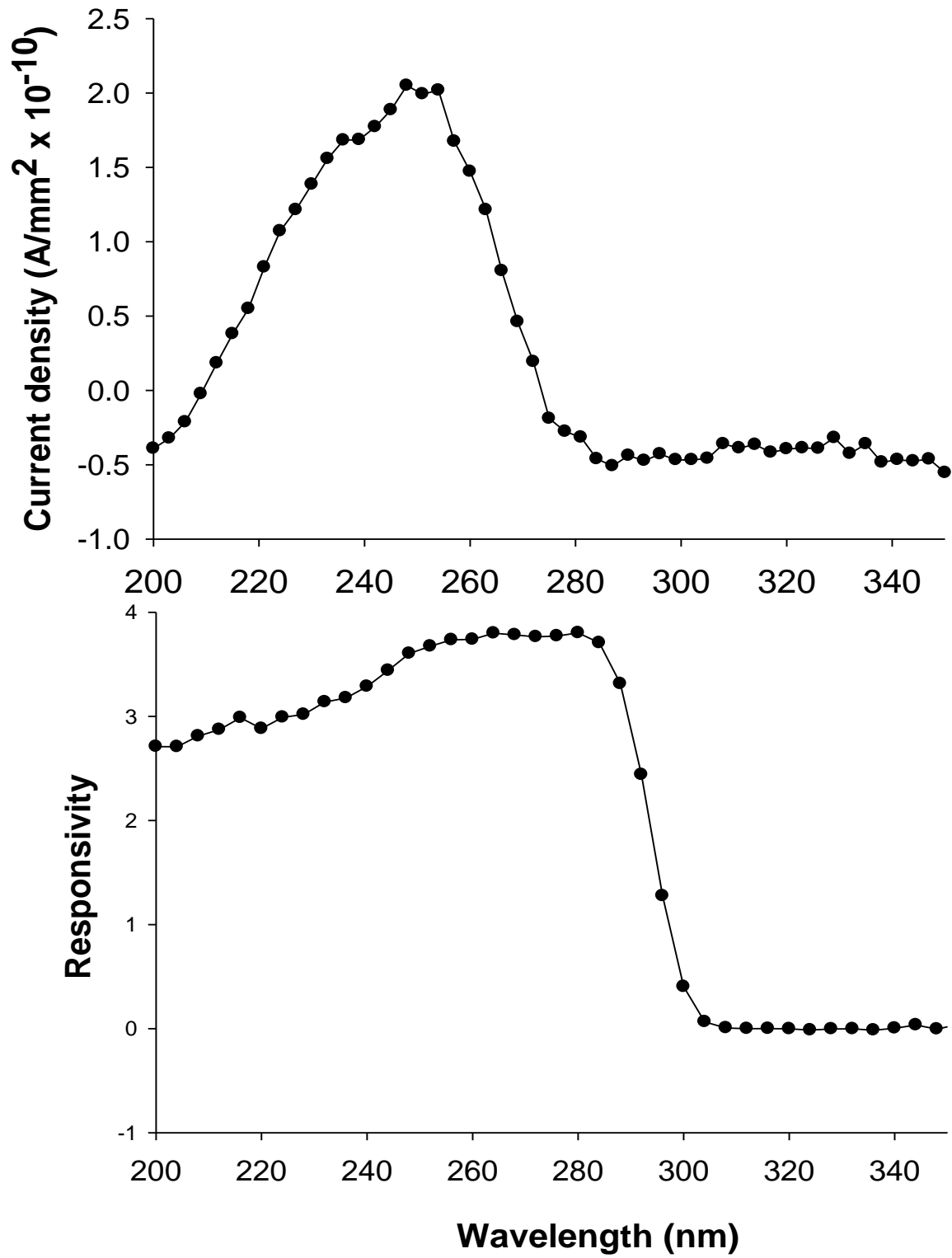


Figure 8.3 (b): AlGaIn photocurrent density response curves as a function of wavelength.

8.4 Conclusions

In conclusion, we have demonstrated the fabrication of visible-blind GaN and solar-blind AlGaN Schottky photodiodes with low zero biased dark currents. Device responsivity as high as 31.8 mA/W for GaN and 3.8 mA/W for AlGaN were recorded. The calculated quantum efficiencies of the photodiodes were 11 % for GaN and 1.7 % for AlGaN respectively. The barrier heights of 0.67 eV and 1.09 were recorded, for GaN and AlGaN photodiodes. The series resistance of GaN was 178 Ω and that of AlGaN 1090 Ω . Ideality factors of 2.48 and 1.35 were recorded for GaN and AlGaN respectively. The commercial and fabricated AlGaN photodiodes have photocurrent density and responsivity maximum peaks occurring in the range of 270 - 280 nm. Further work will be done to improve the performance of AlGaN photodiodes. For the structure studied here, there is a need to etch away the AlGaN and AlN layers so that ohmic contacts are deposited onto GaN.

REFERENCE

- [1] Razeghi M. and Rogalski A., *Journal of Applied Physics*, **79** (1996) 7433.
- [2] Schreiber P., Dang T., Smith G., Pickenpaugh T., Gehred P. and Litton C., *Proceedings SPIE*, **3629** (1999) 230.
- [3] Carrano J. C., Li T., Grudowski P. A., Dupuis R. D. and Campbell J. C., *IEEE Circuit Devices Magazine*, **15** (1999) 15.
- [4] Asif Khan M., Shatalov M., Maruska H. P., Wang H. M and Koukstis E., *Japanese Journal of Applied Physics* **44** (7191) 2005.
- [5] Kida Y., Shibata T., Naoi H., Miyake H., Hiramatsu K., and Tanaka M., *Physica Status Solidi (a)* **194** (2002) 498.
- [6] Wang H-M., Zhang J-P., Chen C-Q., Fareed Q., Yang J-W., and Asif Khan M., *Applied Physics Letters* **81** (2002) 604.
- [7] McCarthy L., Smorchkova I., Xing H., Fini P., Keller S., Speck J., Denbaars S. P., Rodwell M. J. W. and Mishra U. K., *Applied Physics Letters* **78** (2001) 2235.
- [8] Biyikli N., Aytur O., Kimukin I., Tut T. and Ozbay E., *Applied Physics Letters* **81** (2002) 3272.
- [9] Biyikli N., Kartaloglu T., Aytur O., Kimukin I. and Ozbay E., *Applied Physics Letters* **79** (2001) 2838.
- [10] Jiang H., Egawa T., Ishikawa I., Dou Y. B., Shao C. L. and Jimbo T., *Electronic Letters* **39** (2003) 148.
- [11] Motayed A., Davydov A. V., Bendersky A. L., Wood M. C., Derenge M. A., Wang D. F., Jones K. A. and Mohammad S. N., *Journal of Applied Physics* **92** (2002) 5218.
- [12] Butun S., Gokkavas M., Hongbo Y. and Ozbay E., *Applied Physics Letters* **89** (2006) 73503.
- [13] Jhou Y. D., Chen C. H., Chang S. J., Su Y. K., Chang P. C., Chen P. C., Hung H., Yu C. L., Wang S. M. and Wu M. H., *Microelectronic Journal* **37** (2006) 328.
- [14] Su Y. K., Chang P. C., Chen C. H., Chang S. j., Yu C. L., Lee C. T., Lee H. Y., Gong J., Chen P. C. and Wang C. H., *Solid-State Electronics* **49** (2005) 459.



- [15] Sze S. M., Physics of Semiconductor Devices, 2nd Edition, 1981.
- [16] Dereniak E. L. and Growe D. G., Optical Radiation Detectors, Wiley, New York (1984).
- [17] Ozbay E., Biyikli N., Kimukin I., Kartaloglu T., Tut T. and Aytur O., IEEE Journal of Selected Topics in Quantum Electronic **10** (2004) 742.